New insights into the crust and lithospheric mantle structure of Africa from elevation, geoid, and thermal analysis

Jan Globig[(1)], Manel Fernàndez[(1)], Montserrat Torne[(1)], Jaume Vergés[(1)], Alexandra Robert[(2)] and Claudio Faccenna[(3)]

(1) Institute of Earth Sciences Jaume Almera, ICTJA-CSIC, Group of Dynamics of the Lithosphere (G.D.L.), Barcelona, Spain

(2) Géosciences Environnement Toulouse, Observatoire Midi-Pyrénées, France

(3) University Roma TRE, Dept. of Geological Sciences, Italy

Key points:

1) We present 10 min resolution crust and lithosphere maps of Africa constrained by a compilation of seismic Moho data and tomography models.

2) Our maps cover large areas of Africa where no data are available showing 76% fit with seismic data after excluding the Afar plume region.

3) Misfits with seismic data in the Afar region are discussed in terms of residual topography related to sublithospheric processes.

This article has been accepted for publication and undergone full peer review but has not been through the copyediting, typesetting, pagination and proofreading process which may lead to differences between this version and the Version of Record. Please cite this article as doi: 10.1002/2016JB012972

Abstract

We present new crust and lithosphere thickness maps of the African mainland based on integrated modeling of elevation and geoid data and thermal analysis. The approach assumes local isostasy, thermal steady-state, and linear density increase with depth in the crust and temperature-dependent density in the lithospheric mantle. Results are constrained by a new comprehensive compilation of seismic Moho-depth data consisting of 551 data points, and by published tomography models relative to LAB-depth. The crustal thickness map shows a N-S bimodal distribution with higher thickness values in the cratonic domains of southern Africa (38-44 km) relative to those beneath northern Africa (33-39 km). The most striking result is the crustal thinning (28-30 km thickness) imaged along the Mesozoic West and Central African Rift Systems. Our crustal model shows noticeable differences compared to previous models. After excluding the Afar plume region, where the modeling assumptions are not fulfilled, our model better fits the available seismic data (76.3% fitting; RMSE=4.3 km). The LAB-depth map shows large spatial variability (90 to 230 km), with deeper LAB related to cratonic domains and shallower LAB related to Mesozoic and Cenozoic rifting domains, in agreement with tomography models. Though crustal and lithosphere thickness maps show similar regional patterns, major differences are found in the Atlas Mountains, the West African Rift System, and the intracratonic basins. The effects of lateral variations in crustal density as well as the non-isostatic contribution to elevation in the Afar plume region, which we estimate to be ~1.8 km, are also discussed.

1. Introduction

The current crust and lithospheric mantle structure of the African continent results from of a complex, >3.7 billion year old geodynamic history involving: i) juvenile crust formation and craton stabilization during the Archean; ii) extensive crustal reworking during the Proterozoic; iii) Pan-African assemblage followed by Mesozoic break-up of the Gondwana supercontinent; and iv) Cenozoic widespread volcanism, uplift, and continental rifting. The African lithospheric structure has been the target of numerous regional, continental, and global studies, but large parts of the continent still remain unknown because of the lack of seismic studies in vast regions of Africa. Since the first seismic experiments in the Kaapvaal Craton (Willmore et al., 1952) and the East African Rift System (Dopp, 1964), investigation of the crustal and upper mantle structure focused on hotly debated processes shaping the African continent, such as the formation of crust and craton stability during the Archean, the anomalous swell topography (e.g., the African Superswell), the crust/mantle strain partitioning related to the successive tectonic episodes, and the Cenozoic hotspot volcanism and active rifting. The precise knowledge of the current variations of the average density and thickness of the crust and the lithospheric mantle of the different tectonic units throughout the African continent is a major contribution in understanding these processes.

Thanks to an increased number of seismic experiments (e.g., KRISP, EAGLE, MAMBA, Africa-Array, SASE), information on the African crustal structure and its diverse characteristics has improved significantly. However, available seismic data come from stations that are regionally concentrated in four regions, namely the Rif-Tell-Atlas in northern Africa, the East-Africa Rift System, the Kaapvaal-Zimbabwe Craton, and the Cameroon region in west Africa. To bridge data-sparse areas, different regional and continental-scale crustal models exist for Africa or can be developed by extracting this information from global models. The existing crustal models (Table 1), mainly seismological, gravity-based, or some combination of the two, provide homogeneous coverage but show significant differences depending on the modeling technique, the resolution, and the data-type used to extrapolate the seismic estimates to the vast unsampled regions (van der Meijde et al., 2015). Nevertheless, they share the advantage of incorporating a variety of information of

crustal properties with high spatial resolution, allowing the depth of subsurface discontinuities, such as the Moho and the LAB, beneath data-absent regions to be estimated.

First estimates of crustal thickness beneath Africa were taken from global models, based on seismic data compilation (Soller et al., 1982; Cadek and Martinec, 1991). Later, Nataf and Ricard (1996) presented the more developed global 3SMAC model, a tomographic model of the upper mantle, which included a crustal model combined with geophysical and chemical information. The most noteworthy model is the recently published CRUST1.0 gravity-based, global crustal model from Laske et al. (2013), an upgraded version of the previous CRUST2.0 (Bassin et al., 2000) and CRUST5.1 (Mooney et al., 1998) models, where crustal thickness of unsampled regions is statistically inferred according to basement age or tectonic setting. In recent years, CRUST2.0 was the most frequently used model in geodynamic and gravity modeling, and it has also been extensively used for crustal corrections in seismological studies (e.g., Zhou et al., 2006).

Recently, a number of gravity-based global Moho models were presented, which take advantage of the high accuracy and high spatial resolution measurements of the Earth's gravity field and geoid provided by the GOCE and GRACE satellite missions (e.g., Pail et al., 2010). Inverting gravity data for crustal thickness has been used to generate models that are only based on those gravity observations, such as the Veining Meinesz's model by Babherbandi et al. (2013), as well as models that combine gravity observations with seismic data, such as the Delft Moho model (Hamayun, 2014) and the GEMMA model (Reguzzoni et al., 2013). Certainly, these global models have increased our knowledge about crustal structure, but their associated resolution is still too coarse to be applied to regional studies.

New continental-scale Moho estimates beneath Africa, based on gravity modeling, were presented by Tedla et al. (2011) and Tugume et al. (2013). Both studies provide gravity-derived crustal thickness maps, calibrated against seismic Moho estimates and show little variations in crustal thickness between terrains of Archean and Proterozoic age. The crustal model of Tugume et al. (2013) shows overall thinner crust than the Tedla et al. (2011) model for eastern, southern, and central Africa, with differences of more than 6 km for portions of western and northern Africa.

A common feature of the above referenced models is the non-inclusion of the lithospheric mantle in their calculations.

Interestingly, a comparison between existing crustal models for Africa shows remarkable variation in regions were no seismic data are available, especially between global and continental models. Recently, van der Meijde et al. (2015) pointed out that these differences may be up to 28 km in Moho depth, and that gravity-based models actually show less variation between them than that seen when comparing seismic models or combined gravity-based and seismic models. As there is almost no control on the quality of the resulting structure in sparse seismic regions, these authors warn that the impact of these differences for geodynamic interpretation might be significant.

Looking deeper, the structure of the sub-crustal lithosphere beneath Africa is even less well understood. Similar to the Moho maps, the choice of data and approach used has a strong influence on the final model when trying to resolve the poorly constrained topography of the LAB (Eaton et al., 2009). Lithospheric thickness maps for Africa are inferred from global thermal (Hamza and Vieira, 2012; Artemieva, 2006; Artemieva and Mooney, 2001) and seismic models (Priestley and McKenzie, 2013; Pasyanos et al., 2014; Pasyanos, 2010; Rychert and Shearer, 2009; Conrad and Lithgow-Bertelloni, 2006; Plomerova et al., 2002) as well as from continental (Fishwick, 2010; Priestley and Tilmann, 2009; Priestley and McKenzie, 2006; Fairhead and Reeves, 1977) and regional (Fishwick, 2010) seismic models. Perez-Gussinyé et al. (2009) presented a map of the effective elastic thickness beneath the African continent, based on coherence analysis of topography and Bouguer anomaly data. Although most models show a similar trend in lateral thickness variations related to the large African cratons, differences in absolute LAB depth are significant and may be more than 80 km in areas with sparse seismic coverage (e.g., northern Africa) and up to ~50 km even beneath regions that have been studied extensively with seismic investigations (e.g., southern Africa).

Here, we present new insights into the present-day structure of the crust and lithosphere beneath the African continent by mapping lateral variations in Moho and LAB geometry. The goal of the study is to provide crustal and lithospheric thickness maps of the African continent that are consistent with the available seismic estimates

and tomography models, as well as with elevation and geoid data, to ensure their validity on the vast unexplored regions (~80% of Africa). We determine crustal and lithospheric thickness using a combined model of elevation and geoid anomaly data, together with a thermal analysis, under the assumption of local isostasy. The applied methodology includes: i) a comprehensive compilation of existing Moho depth estimates beneath Africa from controlled-source seismic experiments and from receiver function studies; ii) comparison of our calculated crustal thickness with seismic estimates in those regions where they are available; iii) selection of the model parameters that fit better with seismic estimates; and iv) calculation of crustal and lithospheric mantle thickness beneath whole Africa and comparison of our results with recent continental and global-scale models of crustal (Tedla et al. 2011; Laske et al., 2013; Tugume et al. 2013) and lithospheric thickness (Fishwick, 2010; Priestley and Mc Kenzie, 2013). This approach has been successfully applied to image variations in crustal and lithospheric thickness beneath the Atlantic-Mediterranean transition (Fullea et al., 2007), the Arabia-Eurasia collision (Jiménez-Munt et al., 2012), the Iberian Peninsula (Torne et al., 2015), central Asia (Robert et al., 2015), and the southern Indian Shield (Kumar et al., 2014). We discuss the obtained results in terms of major tectonic structures, crust/mantle strain partitioning, and effects of departure from local isostasy.

2. Tectonic background

Africa is mostly an assemblage of Precambrian cratons and fragments, separated by Proterozoic and Paleozoic mobile belts. The continent is currently surrounded by divergent plate boundaries, predefined during Mesozoic break-up of Gondwana and the coeval opening of the Atlantic Ocean, resulting in oblique convergence between Eurasia and northern Africa at a rate of 2 - 6 mm/yr (Nocquet and Calais, 2003; McClusky et al., 2003). Continental break-up and rifting is presently occurring along the boundary between the Nubian and Somalian plates, marked by the 5000 km long East African Rift System (EARS). In the following subsections, we will briefly describe the most remarkable tectonic features, highlighting their significance in relation to Africa's current lithospheric structure and anomalous topographic features. For the sake of simplicity, we will refer to northern Africa as the continental region

extending north from a line between the Central Africa Rift System to the Afar Triple Junction, which coincides offshore with the Atlantic Romanche Fracture Zone that separates the Central and South Atlantic regions. Also, we will refer to southern Africa as the continental region extending south from this line (Fig. 1).

2.1 Archean Cratons

The Precambrian history of Africa can be divided into Archean crust formation and the stabilization of the first cratonic cores, followed by their Proterozoic assemblage, which created the surrounding collisional fold belts. The continent's core is mainly composed of the West African Craton and the Saharan Metacraton, located in northern Africa, Congo Craton, Kaapvaal and Zimbabwe cratons and some smaller Archean fragments, such as the Tanzania and Uganda cratons, located in southern Africa (Fig.1).

In northern Africa, the West African Craton (WAC) and the Saharan Metacraton are separated by the West African Mobile Zone (WAMZ). Archean rocks of the WAC are exposed in the northwestern Reguibat (3.52 - 2.84 Ga) and southwestern Man Leo shields (>3.0 Ga). The center of the less rigid portion of the craton is overlain by the Neoproterozoic Taoudeni Basin, which is a typical intracratonic depression (MacGregor, 1998) filled with ~3 km of Neoproterozoic to Paleozoic deposits. The basin is partly underlain by cratonic basement of the Reguibat Shield and shows regional-scale Pan-African tilting (Mann et al., 2003). To the east, the Saharan Metacraton (Abdelsalam et al., 2002) is a poorly known ~5,000,000 km^2 tract of continental crust. The pre-Neoproterozoic character of its cratonic units suggests a pre-existing Saharan Craton that was remobilized by surrounding Neoproterozoic collision, possibly leading to delamination or convective removal of the negatively buoyant metasomatized cratonic lithosphere (Lucassen et al., 2008; Begg et al., 2009; Shang et al., 2010; Fezaa et al., 2010; Abdelsalam et al., 2011).

In southern Africa, the Congo Craton comprises most of the landmass and is almost entirely surrounded and partly indented by Pan-African foreland belts. The four Archean blocks located at its margins were amalgamated during the Paleoproterozoic, between 2.1 and 1.8 Ga (Fig.1). Large parts of the craton are covered by the Proterozoic Congo Basin (~1.2 million km^2), an intracontinental

depression, filled with 4 to 9 km of Proterozoic to Neogene sediments. The basin experienced very slow subsidence since the Pan-African event, probably due to moderate extension of thick lithosphere (Crosby et al., 2010; Kadima et al., 2011). The long subsidence history (~0.5 Gy) of the Congo Craton, which differs from other sag basins, is not well understood, yet it might be associated either with a downwelling mantle plume (Hartley and Allen, 1994) or with a high-density anomaly within the lithosphere (Downey and Gurnis, 2009).

East of the Congo Craton, the Uganda and Tanzania Cratons are located between the Eastern and Western branches of the EARS. The Uganda Craton, made up of a central Mesoarchean (~3 Ga) and an eastern Neoarchean terrane (~2.5 Ga; Link et al., 2010; Mänttäri et al., 2013), contains Neoproterozoic units that cover the northeastern boundary between it and the Congo Craton. To the south, the ~2.6 Ga Tanzania craton remained stable, whereas the surrounding lithosphere was reworked during several Mesoproterozoic tectonothermal events (Kokonyangi et al., 2006). During the last 80 Ma, kimberlite volcanism has affected the craton (Chesler, 2012).

The Archean core of southernmost Africa consists of the Zimbabwe and Kaapvaal cratons. The Zimbabwe Craton is underlain by Paleoarchean lithosphere, suggesting that isolation from the convective mantle already occurred during the initial phase of craton formation. The last major tectonothermal event that affected the craton occurred at ~2.58 Ga (Jelsma and Dirks, 2002). The Kaapvaal Craton formed and stabilized by accretion of Paleo- to Neoarchean terranes between 3.7 Ga and 2.7 Ga (de Wit et al., 1992; Schoene et al., 2008) and is subdivided into four tectono-stratigraphic terrains (Fig.1). Throughout the Precambrian, the craton was affected by tectonothermal events, and the lithosphere of the southwestern terrain was strongly metasomatized during Mesozoic intervals of kimberlite intrusions at ~110 Ma and ~90 Ma (Pearson et al., 1995; Bell et al., 2005; Kobussen et al., 2008). Formation of the oldest crust in the Zimbabwe Craton occurred between 3.5 to 3.2 Ga, followed by main craton-forming events in the Neoarchean.

2.2 Proterozoic fold belts

African Archean cratons are surrounded by a number of younger Paleoproterozoic,

Mesoproterozoic, and Neoproterozoic mobile belts (Fig.1) formed dominantly by obduction. These tectonic sutures and polycyclic mobile zones created structural basement anisotropies, which often acted as weak zones that were later reactivated during the Phanerozoic and controlled the locus of extension, igneous activity, and initiation of rifting (e.g., Black and Girod, 1970; Thorpe and Smith, 1974; Roberts and Bally, 2012).

Paleoproterozoic belts comprise passive-margin metamorphosed supra-crustal and metasedimentary rocks. Mesoproterozoic belts (e.g., Namaqua-Natal Belt in southernmost Africa) include volcanic arcs and island arc docking, mainly consisting of volcano-sedimentary sequences and gneisses, intruded by Meso- and Neoproterozoic post-tectonic granites. Neoproterozoic belts were formed between ~870 and ~550 Ma during the continent-wide Pan-African orogenic cycle (Kröner and Stern, 2004), which terminated with the amalgamation of Gondwana (~550 Ma). Examples include the Central African Belt, the Mozambique Belt, the Arabian-Nubian shield, the Rockellides and the Mauritanian belts along the WAC and the WAMZ, which include several Archean and Proterozoic fragments, including the Hoggar domain (see Begg et al., 2009 and references therein for a more complete description).

2.3 Paleozoic tectonics

By the end of the Pan-African orogeny (~550 Ma), the African plate formed the interior part of the Gondwana supercontinent, with the modern South American plate to the west and Arabia, Madagascar, India, and Antarctica to the east. Post Pan-African, early Paleozoic molasse-related deposits cover vast areas from west to east Africa and and into southern Africa, filling the Tindouf and Taoudeni basins in the WAC and along the east coast of South Africa (e.g., Cavaroc et al., 1976; Villeneuve, 2005; Milani and De Wit, 2008). During the Ordovician, Silurian, and Devonian, sedimentation in Africa included glacial deposits and post-glacial transgressive shallow marine sedimentation throughout northern Africa and along the southern African coastline.

After a period of Cambrian to Silurian tectonic quiescence, the continent was subject to extensional forces, and the Karoo aged (300 – 190 Ma) basins formed across

Africa. The formation of these basins was controlled by the inherited structures in the underlying Precambrian basement (Catuneanu et al., 2005) and by the combined effect of compression and accretion along the southern margin of Gondwana, with a tensional/transtensional regime propagating into the supercontinent from the Tethyan margin (Wopfner, 2002). During the final amalgamation of Pangea in the Late Proterozoic, convergent activity was limited to the northwestern and southern margins of the African plate, leading to eastward thrusting of the Mauritanian belt (~300 Ma) onto the West African Craton and the formation of both the Variscan orogenic belts (Anti-Atlas) in Morocco, and the Cape Belt (~250Ma) in South Africa. By the end of the Paleozoic, the relief of the continent is supposed to have been relatively flat and low-lying (Doucouré and Wit, 2003), except for the orogenic areas along the margins and broad regions in central and southern Africa, which were affected by mid-Paleozoic deglaciation uplifts (Visser, 1997).

2.4 Mesozoic rift systems

The Mesozoic history of Africa is dominated by episodes of continental rifting related to the break-up of Gondwana. Jurassic and Cretaceous crustal extension events affected huge portions of the African lithosphere (e.g., Burke and Whiteman, 1973; Frizon de Lamotte et al., 2015) most of them reusing pre-existing basement fractures. These fractures initially evolved during Karoo times and resulted in the development of two major rift systems: the West and the Central African Rift Systems (Fairhead, 1988; Fig 1). The eastern African margin was shaped by the fragmentation of East Gondwana in the mid-Jurassic (Royer and Coffin, 1922; König and Jokat, 2010), associated with the opening of the southern Indian Ocean and the southward drift of Madagascar. The break-up of Gondwana left the African continent delimited by passive margins, leading to slow plate rotation and the relative stationary position of Africa since the Mesozoic. Exposed to the effects of episodic deep-mantle upwellings of Mesozoic age (Nyblade and Sleep, 2003), portions of the African lithosphere underwent thermal and chemical modification, which probably induced the bimodal character of the Cretaceous African topography (Doucouré and Wit, 2003).

2.5 Cenozoic tectonics

During the Cenozoic, widespread volcanism affected the African continent, mainly related to Pan-African crustal reactivation (e.g., Ashwal and Burke, 1989), continental rifting (Thorpe and Smith, 1974), and hotspots beneath north-central Africa (Hoggar, Tibesti, Darfur), the Cameroon Volcanic Line (CVL), and the EARS (Fig. 1). The Eocene to Quaternary volcanic fields of Hoggar, Tibesti, and Darfur are marked by topographic swells of broad uplifted Precambrian basement, weakened during the Mesozoic rifting. Their alkaline volcanism might be fed by either unconnected plumes (Wilson and Guiraud, 1992; Burke, 1996), the Afar plume (Ebinger and Sleep, 1998), or by adiabatic upwelling of the asthenosphere in response to the Africa-Europe collision (Bailey, 1992).

The continental interior of West Africa is marked by the onshore section of the ~1600 km long CVL (Fig. 1). Occurrence of mono- and poly-genetic volcanoes, sporadic magma rise, and the lack of age progression along the volcanic centers suggest fossil plume remelting (Halliday et al. 1990), plume-plume interaction (Ngako et al. 2006), decompression melting beneath reactivated shear zones (Fairhead, 1988), or edge-driven convective flow at the northwestern corner of the Congo Craton (Meyers et al., 1998, King and Anderson, 1995; Reusch et al., 2010).

The most striking tectonic and geomorphological feature in East Africa is the seismically and volcanically active EARS (Fig. 1), a large zone of ongoing crustal thinning extending from the Afar triple junction between the Nubian, Arabian, and Somalian plates to the Zimbabwe Craton (McConnell, 1972; Morley et al., 1999; Chorowicz, 2005). Continental break-up along the EARS occurs as rupture of weakened Proterozoic lithosphere (Ring, 1994; Burke, 1996) above a major mantle upwelling (Grand et al., 1997; Nyblade and Langston, 2002; Ritsema et al., 1999; Simmons et al., 2007; Hansen et al., 2012; Hansen and Nyblade, 2013). Two large north-south trending branches circumvent the resistant Tanzania Craton (Fig.1). The eastern branch cuts through Pan-African lithosphere in the Mozambique belt and is connected to the Afar triple junction along the Main Ethiopian Rift (MER, Fig. 1). The MER transects the Ethiopian Plateau, a 1000 km-wide Palaeogene flood basalt province at 2500 m elevation (e.g., Mohr and Zanettin, 1988), which was uplifted after the impingement of the Afar mantle plume on the base of the lithosphere at ~30

Ma (Ebinger and Sleep, 1998). The western branch cuts through Archean basement in the north (Link et al. 2010) and developed along the western border of the Tanzania craton further south. The EARS is an archetypal example of an active rift system (Şengör and Burke, 1978), whose geodynamic origin is under debate. Some studies advocate for one (Afar) plume as the origin of the EARS (e.g., Ebinger and Sleep, 1998; Furman et al., 2004), some advocate for multiple plumes (George et al., 1998; Rogers et al., 2000), and still others advocate for a connection to the African Superplume (e.g., Ritsema et al., 1999; Benoit et al., 2006; Pik et al., 2006; Bastow et al., 2008; Forte et al., 2010; Hilton et al., 2011; Hansen and Nyblade, 2013). Regardless the acting process, any of these mechanisms is causing thermal erosion of the lithosphere, updoming, and dynamic topography.

From Late Cretaceous until recent time, the relative motion between Africa and Eurasia caused transpressive convergence in the northern margin of Africa. As a consequence, the Atlas System, extending from Morocco to Tunisia, was developed during the Cenozoic along zones of crustal weakness inherited from Triassic and Jurassic rifting episodes related to the opening of the Atlantic and Tethys oceans (e.g., Frizon de Lamotte et al., 2000). The Rif-Tell Mountains correspond to accretionary wedges, with fragments of stacked thrust sheets, incorporating high-grade metamorphic rocks and occasional peridotites (Frizon de Lamotte et al., 2000). The Rif-Tell Mountains resulted from the closure of the Tethys Ocean by subduction and further slab(s) retreat, whose polarity and geodynamic evolution is highly debatable (e.g., Vergés and Sàbat, 1999; Faccenna et al., 2004; Rosenbaum and Lister, 2004; Vergés and Fernandez, 2012).

3. Data

To calculate the crustal and lithospheric mantle thickness beneath Africa, we use a methodology based on the integrated modeling of elevation and geoid data, combined with thermal analysis. Seismic data is first used to choose the best reference column to which refer the geoid height, and to define some modelling parameters (see Section 4). The resulting Moho and LAB depth maps are then compared to available seismic data and tomography models and discussed in terms

of the tectonic processes affecting the different region of Africa. In this section, we summarize the data used as model input (elevation and geoid) as well as the seismic data used as constraints.

3.1 Input data: Elevation and geoid

Digital elevation data for Africa were taken from the 1 arc-minute global relief model ETOPO1 (Amante and Eakins, 2009). The high frequency components were removed from the dataset, using a Gaussian low-pass filter with a wavelength of 100 km to avoid mapping unrealistic short-wavelength signals into the modeled Moho and LAB topography related to flexural support of topographic loads. Although included in the calculations, we will not discuss the offshore elevation and bathymetry data further, as we rather focus our observations and investigations on the land surface of the African continent.

Figure 2a shows the topography of Africa, which is distinctly bimodal, dominated by high elevations of >1000 m in eastern and sub-equatorial Africa (A and B in Fig. 2a, respectively), related to the African Superswell, and by average-to-moderate elevations of <500 m in northern Africa and the Congo Basin. Long-wavelength (>1000 km) topographic highs in eastern Africa are related to the Ethiopian and the East African Plateau, both with average elevations of ~ 1500 m, and to the highest rift-related topography (>3000 m) along the flanks of the EARS. In southern Africa, a broad uplifted region surrounds the Cenozoic Kalahari Basin, which is marked by a marginal escarpment related to the highest elevations of > 2500 m.

The relatively low topographic relief of ~ 500 m across northern Africa is mainly related to large-scale flexural sedimentary basins developed in the West Africa Craton (Taoudeni Basin, D in Fig. 2a) and the Sahara Metacraton (Chad Basin, E in Fig. 2a) as well as the Congo Craton to the south (Congo Basin, F in Fig. 2a). To the north, the smooth topography is interrupted by a number of shorter wavelength swells and uplifted regions, such as the Hoggar Massif (~1000 m), the Tibesti Mountains (~ 2000 m) and Darfur (~1200 m; see Fig. 1 for locations). The transition to the passive continental margins of the Atlantic and Indian oceans is marked by coastal areas characterized by low relief (~150 m), with the exception of the northwest corner of Africa, where convergence between Africa and Europe is

marked by high topography (~2000 m) along the Rif-Tell-Atlas orogenic system (C in Fig. 2a) and the southeast and south regions of Africa, where steep topographic gradients mark the transition to the continental shelf (Fig. 2a).

Geoid anomaly data were extracted from the EGM2008 global model (Pavlis et al., 2012). In order to only retain the signature of mass distribution related to the lithospheric structure, we filtered wavelengths exceeding ~4000 km by removing the lower harmonic coefficients from the dataset up to degree and order of 10 (see Root et al., 2014 for a detailed sensitivity analysis of spherical harmonic degrees). The resulting geoid anomalies (Fig. 2b) largely follow the distribution of high and low topography (Fig. 2a). Negative anomalies are generally related to large basins and coastal plain depressions, whereas positive anomalies are related to mountain ranges, domes, and plateaus.

Maximum positive geoid anomalies with values > 12 m coincide with the regions of highest topography (e.g., Atlas Mountains, EARS, Tibesti). The largest long wavelength geoid high coincides with the EARS. With a NNE-SSW direction and a length of > 3000 km, it extends from the Afar Triple Junction, along the MER and increases from ~6 m to ~14 m in the Tanzania Craton. The volcanic centers (Hoggar, Tibesti, Darfur, and CVL) are also related to positive geoid anomalies and high elevation, showing maximum values of >10 m in the Tibesti center and up to 6 m in Hoggar and Darfur. In contrast, the African Superswell is characterized by moderate geoid anomaly values (-4 to +4 m), except in the southwestern border of the Congo Craton and the eastern border of the Kaapvaal Craton, where values of >8 m coincide with high elevation ranges (Fig. 2b).

The most striking feature is the circular geoid low, with a half-wavelength of > 750 km and minimum values of -16 m, located in the center of Africa, associated with the Congo Basin (Fig. 2b). In northwest Africa, a widespread and elongated negative anomaly, with minimum values of -9 m, crosses the WAC, trending NE-SW, parallel to the Atlas. The southwest end of this geoid low extends to the northern and central regions of the Taoudeni Basin, where values less than -4 m are observed. The northeasternmost part of the east Saharan Metacraton is marked by a < -6 m geoid low located in the Nile Delta region. The transition to the continent's margins are characterized by negative anomalies along the eastern coast (Red Sea and Indian

Ocean) and positive anomalies along the western coast (Atlantic Ocean), with the exception of the Gabon and Congo coastlines, where negative values of -4 to -8 m are recorded.

3.2 Seismic estimates

We compiled a comprehensive set of Moho depth estimates throughout Africa and the adjacent Arabian Peninsula from available deep seismic sounding (DSS) and receiver function (RF) studies in order to better evaluate the accuracy of our crustal thickness model. Our total database includes 551 data points: 139 from DSS and 412 from RF, which are regionally concentrated in northwest Africa (Morocco), Arabia, East Africa, Cameroon, and southern Africa. Though the focus of this study is clearly on the crustal and lithospheric structure of the African continent, we considered Moho estimates from Arabia in the evaluation process since throughout most of geological history, the Arabian Peninsula formed part of the pan-Afro-Arabian continent (up until 30 Ma). The compiled seismic data and current knowledge of crustal thickness in Africa is presented in Figure 2c, which displays their uneven distribution and absence of seismic coverage for vast areas of the continent (e.g., WAC, Sahara Metacraton, and Congo Craton). Figure 3 shows that the average crustal thickness resulting from this compilation is 36.58 km, with a standard deviation of 5.79 km with a clear preponderance of values ranging from 34 to 44 km. For a brief review of passive-source seismic studies in Africa, the reader is referred to Fishwick and Bastow (2011). Additional references for both active and passive seismic studies are listed in Table 2.

Crustal thickness estimates from DSS usually have uncertainties ranging from ±3.5 to ±6 km, depending on data quality, modeling, and interpolation techniques (Waldhauser et al., 1998). According to Spada et al. (2013), the vertical error for crustal thickness estimates derived from RF studies ranges from ±3 to ±10 km, with the highest uncertainties expected for complex tectonic areas. Therefore, to benchmark our crustal thickness model, we use a threshold of ±4 km for Moho estimates derived from DSS and ±5 km for those derived from RF studies.

4. Method and model parameters

We map lateral variations in crustal and lithospheric thickness by combining

elevation and geoid anomaly data with a thermal analysis, following the 1-D approach by Fullea et al. (2007). The observed elevation and geoid height are simultaneously fit assuming local isostasy and using a four-layer model composed of water, crust, lithospheric mantle, and asthenosphere. In this context, elevation is proportional to $\int \rho(z)\, dz$, where $\rho(z)$ is the density at a given depth z. The integral extends from the Earth's surface to the compensation level, which is located at 300 km depth, below the deepest point of the LAB over the entire modeled region. In this way, elevation E with respect to sea level can be expressed as (Lachenbruch and Morgan, 1990):

$$E = (\rho_a - \rho_L)/\rho_a * L - L_0 \qquad (E \geq 0)$$

$$E = \rho_a/(\rho_a - \rho_w) * ((\rho_a - \rho_L)/\rho_a * L - L_0) \qquad (E < 0)$$

where L is the total lithospheric thickness, ρ_a is the density of the asthenosphere (set to 3200 kg/m^3), ρ_w is the density of seawater (1030 kg/m^3), ρ_L is the average density of the lithosphere, and L_0 is the depth of the free (unloaded) asthenospheric level (2320 m; Fullea et al., 2007).

Under local isostasy and when lateral density gradients are moderate, the geoid anomaly is proportional to the dipolar moment of the vertical density distribution and therefore is proportional to $\int z\, \rho(z)\, dz$. The geoid anomaly N is calculated by (e.g., Haxby and Turcotte, 1978):

$$N = -2\pi G/g \int z * \rho(z) dz + N_0$$

where G is the universal gravity constant and g is the gravitational acceleration at the Earth's surface. The integration constant N_0, which serves to adjust the zero level of the geoid anomalies, is calculated considering a reference column, where N and the crustal and lithosphere thicknesses and their respective densities, are known.

For the crust, we assume a laterally homogeneous density ρ_C that increases linearly with depth, between predefined values, ρ_S at surface and ρ_B at the base of the crust. The density in the lithospheric mantle ρ_m is considered to be temperature dependent

(e.g., Lachenbruch and Morgan, 1990) such that $\rho_m(z) = \rho_a (1 + \alpha[T_a - T_m(z)])$, where α is the coefficient of thermal expansion, T_a is the temperature at the base of the lithosphere, and $T_m(z)$ is the temperature at depth z in the lithosphere mantle. For the African continent, we can assume that the average mantle is of Archean age; therefore, we have set $\alpha = 3.2 \times 10^{-5}$ K^{-1}, according to Afonso et al. (2005). The temperature distribution with depth is calculated by solving the 1D heat transport equation in steady-state:

$$k \cdot \nabla^2 T + A = 0$$

where k is the scalar thermal conductivity, ∇^2 is the Laplace operator, and A the volumetric heat production. We consider a thermal conductivity of 2.5 W m^{-1} K^{-1} for the crust and 3.2 W m^{-1} K^{-1} for the lithospheric mantle (e.g., Fernandez et al., 1998). The radiogenic heat production is considered to be constant, with values of 0.5 and 0 μW m^{-3} (Vilà et al., 2010; Robert et al., 2015) for the crust and the lithospheric mantle, respectively. The above equation is solved with boundary conditions of fixed temperature at the surface T_s=0 °C and at the base of the lithosphere T_a=1350 ºC (see eqs. 4–32 and 4–33 in Turcotte and Schubert, 2002). For a detailed derivation of the generalized isostasy equation that includes the thermal field in a consistent way, the reader is referred to Fullea et al. (2007).

The choice of thermal parameters influences the calculated Moho temperature, which in turn, modifies the density of the lithospheric mantle. According to Fullea et al. (2007), the calculated LAB depth decreases almost linearly with increasing thermal expansion coefficient and crustal thermal conductivity and with decreasing radiogenic heat production. The calculated LAB depth can vary by ±6 km for a wide range of thermal parameters, whereas the crustal thickness is barely affected (~1 km). The inaccuracy of the calculated crustal and lithospheric thickness associated with the RMSE of the used input datasets is less than 2 and 10 km, respectively, as calculated by Fullea et al. (2007) for the older ETOPO2 (Sandwell and Smith, 1997) and EGM96 (Lemoine et al., 1998) datasets.

4.1 The reference column

Deriving the crust and lithospheric mantle thicknesses from elevation and geoid anomaly data depends on the choice of an appropriate reference column to which

refer these variations and then, from the N_0 value. Determining the reference column for the African continent is not straightforward since it depends not only on the actual crust and lithospheric mantle thickness values (h_c and h_m, respectively) in a given location, but also on the crust and mantle depth-density distribution ($\rho_c(z)$ *and* $\rho_m(z)$, respectively). We can derive h_c from seismic experiments and can calculate h_m from elevation data, considering local isostasy and knowing $\rho_c(z)$ and $\rho_m(z)$. With the thermal approach, we assume $\rho_m(z) = \rho_a (1 + \alpha[T_a - T_m(z)])$ and that the main unknowns are $\rho_c(z)$ and the thermal parameters, which can actually show noticeable variations and uncertainties. Therefore, rather than choosing a reference column for a given location of Africa, we have selected the column that best fits the available crustal thickness data derived from seismic experiments for the whole continent.

Figure 4 shows the fit, in percentage, between the calculated and measured crustal thickness, within an uncertainty of 4-5 km, depending on the type of seismic experiment. The calculated crustal thickness depends on the selected reference column and therefore on the considered average crustal density and the integration constant N_0 in the geoid equation. Fig. 4a shows the fit obtained after considering all the compiled seismic data and illustrates that the fit increases for crustal densities lower than 2810 kg/m^3, leading to fit percentages ranging from 58 and 64%. Low crustal densities (~2750 kg/m^3) are required to match crustal thickness data in the Ethiopian Plateau and the MER, a region overlying the Afar plume and characterized by high elevation (E > 2000 m), positive geoid anomalies (N ~5 m), and moderate crustal thickness. However, the sublithospheric processes beneath the Afar region causes magmatism, transient thermal perturbations, and non-isostatic (dynamic) contribution to elevation. Therefore, we excluded the Afar plume region (i.e., Afar Depression, Ethiopian Plateau, MER, and Kenya Dome) from the evaluation procedure to avoid bias related to this anomalous region. In addition, we excluded results from a RF study by Wölbern et al. (2010) in the Rwenzori Mountain region. The Rwenzori Mountains are located amidst a rift valley in the western branch of the EARS and show high altitudes of >5000 m, high seismic activity (Koehn et al. 2008), and evidence of removal of the lower crust (Wölbern et al. 2010). We repeated our series of test, comparing the results with the thermally-stable parts of the continent, and attained a reasonable range of density (2780 to 2800 kg/m^3) and N_0 (6166 to 6169 m) values that agree well with seismic observations, ultimately increasing the fit

to 76% (Fig. 4b). We will further examine the effects of crustal density heterogeneities and/or mantle contributions to elevation in the Afar area in section 6.

In summary, we chose the best fitting reference column for the African continent, which agrees with 64% of all Moho estimates and with 76% of the data when the Afar plume region is excluded. This column, with elevation at sea level, has an average crustal density of ρ_c = 2790 kg/m^3, a crustal thickness of Z_c = 32.16 km, and a total lithospheric thickness of Z_L = 153.1 km, resulting in a value of N_0 = 6168 m. We emphasize that different pairs of ρ_c and N_0 values might fit the measured crustal thickness data (especially within threshold limits) equally well in terms of fit percentage, but additional seismic constraints on the resulting lithospheric thickness from tomography studies (e.g., Ritsema and van Heijst, 2000; Sebai et al., 2006; Fishwick and Bastow, 2011; Priestley and McKenzie, 2013; see sections 5.3 and 6.2) were used for discrimination.

The average crustal density of 2790 kg/m^3 determined here agrees well with recent gravity field analysis associated with the refined CRUST1.0 model by Tenzer et al. (2015), who found the same average density value for a global average continental crust, including continental shelves and consisting of igneous, sedimentary, and metamorphic rocks. Table 3 compares the compiled crustal thickness values from seismic experiments with those obtained from our model and other previously published global and continental models, distinguishing the cases of using the complete dataset and excluding the Afar region. The maximum difference between seismic data and all models are 13-19 km, regardless of whether the Afar plume region is considered or not, indicating that these differences are not related to this particular region. In contrast, the minimum difference ranges between -17 and -23 km for the whole continent of Africa and between -11 to -16 km when the Afar region is excluded, indicating that modeled crustal thickness exceeds that observed in the Afar area, independent of the model. Our final crustal model has a root mean square error (RMSE) of 6.4 km relative to the seismic estimates, showing the best minimum RMSE (4.3 km) and a maximum fit (76.3%) when the Afar plume region is excluded (Table 3).

4.2 Influence of sedimentary thickness and lateral crustal density variations

To account for lateral changes in crustal density related to the presence of sedimentary basins, we used sediment thickness information from an updated 1ºx1º global sediment thickness map (Laske and Masters, 1997). Since sediment infill decreases the average density of the crustal column and since our approach requires fixing the density values at the top and bottom of the crust, we have calculated the equivalent surface density that would result from a sedimentary layer of thickness h_s and average density ρ_s. In addition, we assume that the density of the sediments and that of the crystalline crust increase linearly with depth and that the density at the base of the sedimentary column coincides with that at the top of the crystalline crust (see Appendix 1). Considering a surface density for the sediments of 2500 kg/m^3, the resulting average crustal density varies laterally from 2760 to 2790 kg/m^3 across the continent, where maximum deviations (30 kg/m^3) occur in regions with > 5 km of sediment accumulation. However, neither the final crustal nor lithospheric thickness maps show significant variations (an observation also made by Tugume et al., 2013) nor a better fit with seismic data when the sediment layers are incorporated.

Another way to evaluate lateral crustal density variations is to use the CRUST1.0 global dataset (Laske et al., 2013). This dataset includes estimated density values for sediments (soft and hard) and consolidated crystalline crust (upper, middle, and lower crust). Thus, average crustal densities vary in accordance with tectonic setting, from about 2700 to 2910 kg/m^3 across the continent, specifically in the large Congo, Taoudeni, and Tindouf basins (~2760 kg/m^3), the WAC (~2790 kg/m^3), the central and southern African cratons (~2780 kg/m^3), the collisional belts (~2820 kg/m^3), and the EARS (~2870 kg/m^3). Interestingly, densities within cratons are between 2770 and 2790 kg/m^3 and therefore are in good agreement with the average crustal density used in our reference column. Additionally, CRUST1.0 provides densities at the base of the crust, ranging from 2890 to 3040 kg/m^3, with higher density values assigned to Phanerozoic basement (~3000 kg/m^3) and to the Cenozoic rifts (~3040 kg/m^3). Therefore, knowing the average and bottom crustal densities, the 2D lateral density structure from CRUST1.0 is incorporated into our analysis using Eq. (A.5) to adjust the density at the surface of our model. The resulting changes in the average

crustal density relative to the initial value of 2790 kg/m^3 range from -290 to +120 kg/m^3, with maximum negative and positive differences restricted to the northeastern African margin and the northern portion of the EARS, respectively. Nevertheless, for the majority of the continent, the changes in density range from -60 to +55 kg/m^3. The incorporation of these changes in crustal density improve the calculated Moho depth in some regions (e.g., in the northern Zimbabwe Craton and Witwatersrand Block of the Kaapvaal Craton). However, the fit obtained using all the seismic observations decreases to ~41% and the fit obtained when the Afar region is excluded decreases to ~54.75%.

5. Results

In this section, we compare our results with estimates from seismic experiments, focusing on seismically well-sampled regions (i.e., Morocco, Cameroon, East Africa, and southern Africa), and we present our crustal and lithospheric thickness maps for Africa. The complete parameter setup and input values used are outlined in Table 4. The calculated crustal and lithospheric thickness values were projected onto 10 arc-min grids in order to resolve features that are within the resolution of the input EGM-2008 geoid data (spherical harmonics developed until degree and order 2159, Pavlis et al., 2012).

5.1 Comparison with seismic Moho depth estimates

Our crustal thickness results across Africa are in overall good agreement with those from seismic investigations. At regional scale, good fit is observed in Morocco, Tunisia, the Arabia-Nubian Shield, along the CVL, and in the Tanzania, Zimbabwe, and Kaapvaal cratons (Fig. 5a). It is worth noting that the predicted crustal thickness values largely exceed the observations in the region affected by the Afar plume and the EARS, with deviations of > 10 km (Fig. 5b). The degree of fit between modeled and observed crustal thickness is summarized in Table 3, where our results show increase fit with seismic estimates (from 61% to 76.3%) when the Afar plume region is excluded. This anomalous region includes most of the EARS with the MER and the Ethiopian Plateau, the Eastern Rift branch and the Kenya Dome, and the Turkana Basin, where larger extension in the northern Kenya Rift leads to stronger

crustal thinning (up to ~21 km, Gajewski et al., 1994). The excess crustal thickness predicted in this region is due to the fact that the hypotheses of our approach are not strictly valid. That is, the given assumptions do not apply to portions of lithospheric mantle affected by the Afar plume, which causes magmatism, dynamic uplift, and transient thermal regime (see Discussion).

Nevertheless, we also observe higher than expected crustal thickness differences for stations located outside the Afar plume region. In west and southern Africa, misfits exceeding by few km the seismic uncertainties (4 - 5 km) are observed in the WAC as well as in the Namaqua-Natal Mobile Belt and northern Kaapvaal, respectively. Some of these misfits coincide with areas where shear wave velocity profiles indicate either unclear Moho signals or multiple Moho detections (e.g., in the Kaapvaal Craton, Kgaswane et al., 2009) thus suggesting that the uncertainties associated with seismic estimates can exceed 5 km in these cases. Therefore, our calculations could be within the range of measured values and do not allow for firm conclusions on the validity of the modeling assumptions.

In northern Africa, comparison with seismic data in the Rif (northern Morocco) is somewhat ambiguous. Misfits of > 5 km occur along the north-south direction of the wide-angle seismic profile by Gil et al. (2014) located in the external zone of the Rif, where crustal thickening is observed. However, our results are in good agreement with RF estimates from Mancilla et al. (2012) in the same area. In contrast, in the region affected by crustal thinning beneath northeastern Morocco, our model shows misfits > 5 km with RF (Mancilla et al., 2012), but good agreement with the estimates from DSS (Gil et al., 2014). Thus, differences in our model of > 5 km compared with seismic estimates in the Rif cannot be ascertained as they are well within the range of values coming from two independent experiments. These discrepancies are related to the complex Neogene tectonic evolution of the Iberia-Africa plate boundary, where several deep-seated processes, such as mantle delamination, slab retreating, and lateral slab tear, can interact (e.g., Spakman and Wortel, 2004; Faccenna et al., 2004; Vergés and Fernandez, 2012; Bezada et al., 2013; Mériaux et al., 2015; Miller et al., 2015; Mancilla et al., 2015).

Figure 6 summarizes the degree of fit (in percent) between the modeled and observed crustal thicknesses for the whole continent, the whole continent excluding

the Afar plume region, and for different regions in which data can be grouped. A positive/negative mismatch indicates under/over calculated crustal thickness, respectively. In the Afar plume region, the calculated values are clearly overestimated due to the influence of the sublithospheric mantle activity (see Discussion). In the other regions, calculated values reproduce the observations well, with mean mismatches between -0.52 and +0.15 km. We note that excluding the Afar plume region results in a much better fit, with a mean mismatch of -0.37 km and a standard deviation of 4.32 km (Fig. 6).

5.2 Crustal thickness map

Figure 7a shows the calculated crustal thickness map for Africa. The circled area in the northern EARS denotes the region affected by the Afar mantle plume, where the hypotheses of our method are not completely fulfilled. Modeled crustal thickness varies from minimum values of 28-30 km along the Atlantic coastal zone, particularly in northern Africa, to maximum values of ~48 km in southern Africa, particularly beneath the Tanzania and Kaapvaal cratons. Significant variations in Moho geometry appear to be sensitive to the large-scale tectonic framework of the continent but also occur within the boundaries of distinct tectonic regions (e.g., Saharan Metacraton, WAC, Congo Craton, Rif-Tell-Atlas Alpine System; Fig. 7b). Overall, thick crust (>37 km) is associated with Archean cratons and shields and with Proterozoic belts. Crustal thicknesses higher than 40 km are observed within the southern African cratons, Phanerozoic mountain belts, and single dome structures related to hotspots in northern Africa (Fig. 7). The crustal model depicts a bimodal distribution, with a clear north-south division, and distinct crustal structure and thicker cratonic crust in southern Africa (38-44 km) compared to the northern half of the continent (33-39 km).

In northern Africa, maximum crustal thickness values (42 km) correspond to the WAC and to the northern part of the WAMZ. A noticeable crustal thinning towards the western and southern margins of the WAC is imaged, with values of 32-36 km in the Reguibat and Man-Leo shields (Fig. 7). The most striking feature is the conspicuous NNE-SSW oriented crustal thinning (from 28 to 34 km) separating the western and eastern northern-Africa regions. This thinning cross-cuts the Sahara Metacraton, running between the Murzuq and Al Kufrah cratons, and apparently

connecting the CVL, the Tibesti hotspot, and the Haruj volcanic field (Fig. 7b). Our model also shows that the Chad Craton is affected by crustal thinning, with Moho depths of ~32-34 km. Towards the east (i.e., the Al Kufrah Craton and Arabian-Nubian Shield), the crustal thickness increases to 35-39 km.

In southern Africa, our model depicts a more homogeneous crustal structure. Regional crustal thickness values are about 40-42 km, thinning very abruptly towards the western and southern margins and more gently towards the eastern margin. In the Congo, Uganda, and Tanzania cratons, crustal thickness is between 36 - 43 km, agreeing well with seismic Moho estimates for these regions (e.g., Sandvol et al, 1998; Tokam et al., 2010; Tugume, 2011). Maximum crustal thickness values exceeding 46 km are found in the Kaapvaal Craton. East of the Tanzania Craton and along the eastern branch of the EARS, crustal thickness ranges between 30 - 34 km.

The Proterozoic intracontinental basins are marked by greater crustal thickness. Both, the Taoudeni and the Congo basins are located in the central parts of the WAC and Congo Craton, where our model shows the thickest crust, with values of 38 and ~43 km, respectively.

5.3 Lithospheric thickness map

The resulting lithospheric thickness or LAB-depth map (Fig. 8a) shows large spatial variability, with values ranging from 90 - 230 km. Overall, the distribution of thick lithosphere correlates well with the tectonic boundaries of the large African cratons and with geoid minima (Fig. 2b). Thin lithosphere is observed along the coastal regions of the Atlantic Margin, the central part of northern Africa, and the eastern branch of the EARS, coinciding with geoid maxima (Fig. 2b). In the region affected by the Afar mantle plume (circled area in Fig. 8a), results are not reliable due to the above mentioned limitations. Unlike for the crust, the LAB depth map does not show a bimodal distribution between northern and southern Africa but instead, lithospheric thickening and thinning appears to be associated with cratons and mobile belts and with Mesozoic and Cenozoic extension, respectively (Fig. 8b). In the WAC, the lithosphere thickness varies from 110 km beneath the Man Leo Shield to the south to ~200 km beneath the northern part of the craton. Thick lithosphere in northwest Africa is not limited to the WAC but extends to the northeast into the northern

segment of the WAMZ, with values exceeding 200 km. Beneath the Taoudeni Basin, the lithosphere thickens from 140 to >200 km following a southwest-northeast trend. A similar pattern with thick lithosphere extending far into the Sirt Basin is also indicated by positive S-wave anomalies between 150 and 200 km in global (Lebedev and van der Hilst, 2008) and continental surface-wave models (Ritsema and van Heijst, 2000). Our modeled lithosphere beneath the WAC is, on average, 165 km thick, with values up to 200 km, which is in good agreement with surface wave tomography estimates (Sebai et al., 2006). It must be noted that depth-variations of seismic velocities, particularly in S- and surface waves, can be interpreted in terms of lithospheric thickness tough they strictly are indications of speed. Then, the comparison between seismic and thermal lithosphere is not straightforward due to the effects of attenuation, partial melting, and rheology changes between the conductive lithosphere and the underlying convective upper mantle on the seismic velocities. Thick lithosphere (> 160 km) in the Sahara Metacraton is limited to its northeastern portion, coincident with the Al Kufrah Craton, with maximum thickness of 190 km (Fig. 8). These values are consistent with continent-scale seismic studies, imaging fast velocities down to 150 (Ritsema and van Heijst, 2000) and 180 km depth (Sebai et al., 2006) beneath this region. In the southern portion of the Metacraton, including the Chad Craton, the lithosphere thickens from 130 km in the west to 160 km in the east. S-wave tomography shows a similar trend, with increasing velocity perturbations between 100 and 175 km depth oriented in a west-east direction (Begg et al., 2009). Overall, the western half of the Saharan Metacraton shows a relatively thin lithosphere (110-140 km) coinciding with the CVL, the Tibesti hotspot, and the Haruj volcanic province, which also separates the WAC from the Congo Craton (Fig. 8b).

In southern Africa, the Congo Craton is underlain by the thickest lithosphere (170-220 km) obtained in our model. This is in good agreement with previous seismic models, proposing a maximum lithospheric thickness of 230 km beneath the center of the Congo Basin (e.g., Pasyanos and Nyblade, 2007; Pasyanos, 2010; Fishwick, 2010). The fact that the thickest lithosphere in Africa is related to the Congo Craton, especially to the Congo Basin area, is a common feature in seismic tomography, suggesting a deep cratonic root, down to depths of 200-250 km (Ritsema and van Heijst, 2000; Sebai et al., 2006; Priestley et al., 2008; Begg et al., 2009) and

supports our results. The thick lithosphere extends to the south-southeast towards the Kalahari Craton and the Damara and Zambezi belts, with values of 170-190 km. Similar values are found in the Zimbabwe and Kaapvaal cratons and in the Mesoproterozoic Namaqua-Natal Belt.

On average, the Kaapvaal Craton lithosphere is ~170 km thick, which appears to be rather thin compared with LAB depths inferred from body-wave studies, which show high velocity roots down to 200 km (Ritsema and van Heijst, 2000), if not 300 km (James et al., 2001; Fouch et al., 2004). Surface wave and receiver function studies also indicate very thick lithosphere, down to ~300 km (Chevrot and Zhao, 2007; Wittlinger and Farra, 2007). In contrast, a number of seismic studies argue for a thinner lithosphere beneath the southern and central Kaapvaal Craton, as they image a fast mantle lid down to 160-180 ± 20 km (Li and Burke, 2006; Priestley, 1999, 2006, 2008) and display a distinct low-velocity zone beneath 150 km (Savage and Silver, 2008; Wang et al., 2008; Vinnik et al., 2009), as well as a change in anisotropy (Freybourger et al., 2001) and LAB conversions at ~155 km depth (Hansen et al., 2009). Chemical tomography from Begg et al. (2009) shows the base of depleted lithosphere varying from ~150 to 200 km depth, whereas LAB-depth estimates of 150 to 170 km are inferred from heat flow and geothermobarometry on kimberlitic xenoliths (Jones, 1988; Rudnick and Nyblade, 1999; Artemieva and Mooney, 2001; Deen et al., 2006; Priestley et al., 2006). Therefore, our results agree well with minimum lithosphere thickness estimates in the Kaapvaal Craton and thus appear to be fairly reasonable. Moreover, we observe a slightly thinner lithosphere (~150 km) along the western boundary of the Kaapvaal Craton, towards the northwestern Namaqua-Natal Belt, which is also indicated by low-velocity anomalies at 150 km depth in the regional P- and S-wave models of Fouch et al. (2004).

Figure 9 shows two lithospheric profiles crossing the African continent, in both a north-south and northeast-southwest orientation. These profiles display evidence for different deformation styles between the crust and lithospheric mantle. Although the regional patterns of crust and lithospheric thickness look similar, major differences are delineated in the Atlas region (northeast-Morocco), where the crust is relatively thick compared to the lithospheric mantle (e.g., Zeyen et al., 2005; Teixell et al., 2005; Fullea et al., 2007). Similar deviations are seen near the CVL and the Tibesti

and Haruj volcanic fields, where the crust is relatively thin compared to the lithospheric mantle. The intracratonic basins (e.g., Congo Basin and Taoudeni Basin) display remarkable lithospheric mantle thickening. Despite the fact that the dominant contribution to the geoid is generally related to topography, Figure 9 shows large departures in the regional trends of elevation and geoid along both profiles, especially in the central Africa region. The smooth Moho geometry results in a LAB depth that mimics the geoid variations, such that the higher the geoid, the shallower the LAB.

6. Discussion

Our crustal and lithospheric thickness model is based on a set of assumptions that, in some places, might not apply due to the complex nature of the crust-mantle system. Apart from the simplifications required by our methodology concerning the crust and lithospheric mantle densities, the strongest assumptions are those related to local isostasy and a steady-state thermal regime. For wavelengths on the order of tens to hundreds of kilometers, depending on the effective elastic thickness and vertical load distribution, local isostasy is an acceptable approximation (e.g., England and Molnar, 1997; Watts, 2001; Turcotte and Schubert, 2002), and thermal equilibrium is particularly fulfilled in old tectonothermal provinces. Hence, lithosphere thermal equilibrium is valid across most of the study area. In regions affected by transient temperature conditions, due to lithosphere thinning or thickening, steady-state thermal modeling tends to overestimate or underestimate the actual lithospheric thickness, respectively, and to minimize the LAB depth variations. Therefore, the results of our model should be interpreted as the physical conditions needed to produce the required density distribution rather than as the actual thermal boundaries (for more details, see Fullea et al., 2007; Robert et al., 2015).

In addition to the above mentioned assumptions and limitations, there is the contribution to topography associated with the transmission to the Earth's surface of viscous vertical stresses produced by sublithospheric mantle convection, the so-called dynamic topography. In that case, the assumption of isostasy, either local (Airy) or regional (flexure), is not accomplished. The dynamic topography signature

of the African continent has been the subject of a vigorous debate over the last decade. The fundamental observation, inspired by the seminal work of Burke (1996), is that a surge of intraplate volcanism and of uplift and subsidence shaped the African continental topography during the last 30 My. Since then, a number of studies have tried to quantify the contribution of vertical motion on the African topography and whether this may be related to mantle dynamics. For example, several studies proposed that large-scale, deep-mantle dynamics under the African plate are dominated by the influence of a superplume located under southern Africa (Hager et al., 1985; Silver et al., 1988; Lithgow-Bertelloni and Silver, 1998; Behn et al., 2004, Gurnis et al., 2000; Conrad and Gurnis, 2003; Forte et al., 2010; Moucha and Forte, 2011).

To ascertain the amplitude of dynamic topography is a complicated task and, in general, it has been done with two different approaches. The first uses a direct conversion from free air gravity to an estimated topographic effect resulting from dynamic forces on the base of the plate using a 50 mGal/km conversion, assuming a mantle density of 3300 kg/m^3 (Craig et al., 2011). This approach shows localized dome-shaped positive features distributed over the entire continent, particularly associated with the EARS (about 500 m), between the Ethiopian and Kenya dome, and also with the South Africa and Angola dome (up to 700 m), as well as Hoggar and Tibesti and in the Atlas. Negative anomalies are well marked in the Congo basin (up to 500 m) and in the El Djouf–Erg. The second approach uses large-scale tomography to deduce mantle flow and to compare with residual topography (Le Stunff and Ricard, 1995; Hager et al., 1985; Forte 2007). More recently, joint inversion approaches have been carried out between global seismic and surface geodynamic datasets, including geoid, gravity, and topography anomalies as well as surface plate motions (Simmons et al., 2009; Forte et al., 2010). The latter approach shows small dynamic topography in South Africa, a remarkable positive anomaly around the Ethiopian-Yemen dome, and negative anomalies associated with downwelling in the Egypt and Congo basins. Moucha and Forte (2011) investigated the origin of the Congo Basin negative anomaly, concluding that it may be related to both a dense anomaly in the deep lithosphere (Buiter et al., 2012 and this work) and the convective drawdown driven by surrounding deep mantle upwellings. Different results in terms of amplitude of dynamic topography obtained by different

methodologies (e.g., Craig et al., 2011 vs. Forte et al., 2010) recently raised skepticism on the role mantle dynamics have on surface topography (Molnar et al., 2015).

It is worth noting that the only region where the difference between calculated and measured crustal thickness clearly exceeds the accepted uncertainties (4 – 5 km) is the Afar plume region, therefore substantiating the contribution of dynamic topography (section 6.4). This does not imply that in other regions the model assumptions are strictly fulfilled but that the encountered differences, even exceeding the uncertainty range, could be explained by variations in the average crustal density related to sediment thickness, magmatic intrusions, and/or underplating (section 6.3).

In this section, we evaluate the significance of our results for Africa in terms of: 1) previous global and continental-scale models of crustal and lithospheric thickness; 2) contributions from processes modifying the average crustal density; and 3) contributions of dynamic topography in the Afar plume region.

6.1 Comparison with crustal models

As mentioned previously, several crustal models are available for Africa, based on different methods and input data (Table 1). Instead of an extensive comparison, we decided to compare our crustal thickness map with the global-scale CRUST1.0 model, as it is the most widely used among the modeling community, and with two gravity-derived continental-scale models, namely Tedla2011 and Tugume2013 (Figure 10). A Bouguer anomaly map from Pérez-Gussinyé et al. (2009) is added to provide additional qualitative information on lateral density variations within the crust and on Moho topography. Table 5 summarizes the differences between the above referenced models and our model. The model with the minimum difference is Tugume2013, with a RMSE of 4.04 km. We note that although the RMSE varies between 4.04 and 4.95 km for all comparison models, the minimum and maximum crustal variations range from +16.7 to -26.5 km, indicating that, at some regions, differences can be pronounced.

A comparison with CRUST1.0 shows that our results lie within ±2 to ±4 km for most areas of the continent and that the largest differences (> 6 km) are concentrated in

five regions (Fig. 10a). Our crust is significantly thicker than CRUST1.0 in the Mediterranean margin, the EARS, and in the Kaapvaal Craton while our crust is thinner towards the west and south of the WAC and particularly along the West African Rift, extending from the CVL to the Tibesti hotspot and the Haruj volcanic field.

The largest differences related to the EARS region are due to the limitations of our approach. However, overestimation of crustal thickness in our model relative to CRUST1.0 is not restricted to the Afar plume region, but it extends further north along the Red Sea margin and to the south along the branches of the Eastern and Western rift valleys. These differences are most likely related to the fact that the current thermal regime and regional mantle conditions depart from the assumption of thermal steady-state and isostatic equilibrium.

Large differences (> 8 km) are also observed along the Mediterranean margin (Fig. 10a), and it is difficult to identify the cause as our model well fits the few available seismic data at the eastern Mediterranean coast (Fig. 5a). CRUST1.0 is based on one-degree averages of crustal thickness from DSS and RF studies, and Moho depth is calculated from gravity constraints where no seismic data exist. In regions lacking both, seismic and gravity constraints, crustal thickness is extrapolated based on statistical averages of crustal properties (e.g., basement age, tectonic setting). The thicker crust in our model might be related to the different input densities used, since in the CRUST1.0 model the crustal type for northern Libya and Egypt is defined as 'extended crust' with very low average crustal density (< 2700 kg/m^3).

In the southernmost African cratons, our crust is, on average, 4-6 km thicker than that of CRUST1.0 but not in the surrounding Proterozoic belts. Our modeled crustal thickness (38-44 km) agrees well with most seismic estimates across southern Africa, where measured Moho depth is between 35 and 50 km in the Kaapvaal and Zimbabwe cratons (e.g., James et al., 2003; Kwadiba et al., 2003; Nair et al., 2006; Niu and James, 2002; Youssof et al., 2013). Yet, our model is not able to predict the extreme short-wavelength variability in Moho depth beneath the various tectonic blocks in southernmost Africa, such as those observed by Youssof et al. (2013).

The most outstanding differences, however, are along the western and southern

edges of the WAC and along the Cameroon-Haruj lineament, where CRUST1.0 suggests crustal thickening and where our model predicts crustal thinning (Fig. 10a). Similar results are obtained in a comparison with the Tedla2011 model, but not with other gravity-based (e.g., Bagherbandi et al., 2013; Tugume et al., 2013) and seismological crustal models (Meier et al., 2007; Pasyanos and Nyblade, 2007). Moho estimates from RF (Kosarian, 2006) and DSS (Klingelhoefer et al., 2009) show crustal thicknesses of 26 - 28 km in the West African margin that along with a long-wavelength, north-south orientated Bouguer anomaly around 0 mGal, give support to our results (Fig. 10d). Similarly, our results question the crustal thickening suggested by CRUST1.0 along the Cameroon-Haruj lineament, which largely coincides with the Mesozoic West and Central African Rift System (WCARS). Unfortunately, there are no seismic constraints on the crustal structure in these regions, but the relative Bouguer anomaly high (~10 to -30 mGal) in Nigeria and Niger (Fig. 10d), together with spectral studies of gravity data, indicates a reduction in crustal thickness beneath the western portions of the Saharan Metacraton (Okereke, 1984; Fairhead, 1986; Fairhead and Okereke, 1987; Fairhead and Green, 1989). Moreover, Fairhead (1986) pointed out that in contrast to other rifts, the evolution of the WCARS is primarily characterized by subsidence and that the amount of extension is at least four times greater than in the western and central Kenya rifts. We therefore argue that the crustal thinning observed in our model beneath the Mesozoic rift systems is a likely feature.

Overall, our model is in good agreement with Tedla2011, but differences in crustal thickness show an apparent undulating pattern (Fig. 10b). Along the Mauritanian Belt, the Nigerian margin, and the northern portion of the Saharan Metacraton, these differences are similar to those previously discussed with CRUST1.0. Likewise, for the Ethiopian Plateau, the Tanzania Craton, and the center of the Congo Craton, our model shows a thicker crust. Tedla et al. (2011) performed a gravity Euler deconvolution to estimate the Moho depth at a resolution of 0.25º, but the application of this method and its validity to the African continent has been questioned (Reid et al., 2012; van der Meijde and Nyblade, 2014). The technique is based on using the spectral content of the gravity field to detect subsurface interfaces, and it is especially problematic along continental boundaries or in regions with significantly thinned crust (van der Meijde et al., 2015). Additionally, the thinnest crust in the

Tedla2011 model is around 33.25 km, indicating a cut-off in the Euler solutions at this depth (Tugume et al., 2013). Tedla et al. (2011) did not consider seismic data to benchmark their crustal model.

The comparison with the Tugume2013 model shows that we obtain an overall thicker crust, with differences ranging from 0 - 4 km for most of the African continent (Fig. 10c). The model of Tugume et al. (2013) is based on a 3D Parker-Oldenburg iterative inversion (Oldenburg, 1974; Parker, 1973) of EIGEN-6C gravity data and predicts a relatively flat and thin crust (28-34 km) for north, west and central Africa and a thicker crust (36-40 km) in southern Africa. Major differences with our model (below -4 km) are observed along a southwest-northeast oriented corridor, running from the central regions of the WAC to the northeast regions of the Atlas Mountains, along the northernmost regions of the Sahara Metacraton, the northern coastal zones of the Nubian Shield, and the Congo Basin. Locally thinner crust is also seen in southern Africa and in East Africa (e.g., in the flanks of the Ethiopian Plateau). In the Afar Depression and in the central and southern regions of the EARS, the Tugume2013 model shows similar mismatches than our model, relative to the seismic estimates and the CRUST1.0 and Tedla2011 models.

In a recent review of global and continental crustal models, van der Meijde et al. (2015) showed that all models have thick crust in western and northern Africa, indicating that crustal thickness is rather underestimated in Tugume2013. In addition, the spatial extent of negative differences with our model (Fig. 10c) mimics the distribution of thick sediments (> 4 km) inferred from the global sediment model (Laske and Masters, 1997), which was used by Tugume et al. (2013) to correct the input gravity signal for sedimentary basins. Hence, the resulting effect of the correction proposed by Tugume et al., (2013) on Moho topography might not be valid for terranes that underwent intracratonic basin formation, especially in those areas where detailed information on sediment thickness and basin structure is missing and its geodynamic evolution is debatable (e.g., in the Congo Basin; Hartley and Allen, 1994; Downey and Gurnis, 2009; Crosby et al., 2010).

6.2 Comparison with lithospheric models

In this section, we compare our lithospheric thickness map for Africa with a

continental model from Fishwick and Bastow (2011) and with a global model from Priestley and McKenzie (2013), both of which are based on surface-wave tomography. Hereafter, these models will be named FB2011 and PMK2013, respectively (Fig. 11). Comparing estimates of lithospheric thickness is a complex task as the LAB does not correspond to a seismically detectable change in composition but rather to a rheological boundary. The nature of this boundary is elusive and debatable in terms of its properties (e.g., Artemieva, 2009; Eaton et al., 2009; Artemieva, 2011). Especially beneath cratons, its rheological characteristics might change over a thick zone, ranging from 20 km in the presence of fluids to 50 km in dry conditions (Eaton et al. 2009). Therefore, we prefer a qualitative comparison between our results and those from the FB2011 and PMK2013 models, focusing on regional changes in the lateral lithosphere structure beneath Africa. The depth to the LAB in these models was obtained by converting velocity variations to temperature estimates and further to lithospheric thickness estimates using empirical relationships between velocity, pressure, and temperature (Priestley and McKenzie, 2006). Special caution interpreting these models is recommended, as velocity anomalies of non-thermal origin may account for up to +3% of Vs amplitude caused by variations in chemical composition and/or to the presence of melts/fluids (e.g., Artemieva, 2009; Afonso et al., 2010). Furthermore, differences between our results and these models may be related to their spatial resolution and vertical uncertainties. Usually, the horizontal resolution of these models allows features on the order of 200-250 km to be recovered, with a vertical resolution of 25-50 km (Fishwick and Bastow, 2011; Priestley and McKenzie, 2013).

Surprisingly, a comparison among the three models shows that the overall pattern of thick lithosphere is very similar, especially beneath the cratons (Fig. 11). All models exhibit a thick lithosphere (> 160 km) beneath western, central, and southernmost Africa and thinner lithosphere (< 140 km) beneath the Atlas region, the CVL, the WCARS, the Saharan Metacraton, and along the Atlantic margins. In the WAC, our model shows a thick lithospheric root beneath the Taoudeni Basin, which agrees well with the observations in both the FB2011 and the PMK2013 models. Another common feature in all models is the extension of thick lithosphere towards the northeast, across the boundaries of the WAC, paralleling the Atlas Mountains. As this thickening is also observed in our crustal model (Fig. 7) both thick crust and

lithosphere might be a realistic feature in this region. Compared to FB2011, the lithospheric thinning along the western boundary of the WAC is more pronounced in our model and in PMK2013, where these two later models show thinner lithosphere beneath the Neoproterozoic Mauritanian Belt relative to the WAC.

Large variations in lithospheric thickness are visible beneath the Saharan Metacraton in our model and the FB2011 model, but not in PMK2013 (Fig. 11). Indeed, PMK2013 shows almost no variations in lithospheric structure beneath northeastern Africa, which might be related to the parameterization used to estimate the LAB-depth and/or the limited vertical resolution of the model (see Priestley and McKenzie, 2013 for details). The observed lateral thickness variations in our model and in FB2011 are of similar amplitude (~ 80 km) and seem to be related to the remnants of the pre-Neoproterozoic Saharan Craton, the Mesozoic rifts, and the Cenozoic volcanic provinces.

Furthermore, all three models show a north-northeast and an east-northeast trend in lithospheric thinning along the WCARS, extending from the CVL towards the Haruj volcanic province and the Darfur hotspot, respectively, and coinciding with crustal thinning. According to Fairhead (1988), the over 8000 km long WCARS has a consistent geological and geophysical expression that is best explained by lithospheric extension accomplished by ductile flow of the lower crust and upper lithospheric mantle, as quantified by McKenzie (1978) and by Jarvis and McKenzie (1980). Though our absolute lithospheric thickness is around 30-40 km thicker in the WCARS compared to the FB2011 and PMK2013 models due to the differences between thermal and seismic LAB definitions and the vertical resolution, the impact of the tectonic processes caused by large-scale Mesozoic extension on the lithospheric structure are well expressed in our results in both the crustal and lithospheric thickness maps (Figs. 7 and 8).

Our model is in good agreement with the lithospheric variations across the Congo Craton seen in FB2011 and PMK2013 and also with lithosphere thickness estimates of ~210 km from kimberlitic garnet xenocrysts (Batumike et al., 2009). A decrease in thickness to the south of the Congo Craton is visible in all models (i.e., our model, FB2011, and PMK2013), but this thinning is more pronounced in the PMK2013 model. The Tanzania Craton is affected by continental rifting, possibly associated

with a mantle plume (Nyblade and Robinson, 1994; Simiyu and Keller, 1997; Prodehl et al., 1997; McNutt, 1998; Ritsema et al., 1999; Weeraratne et al. 2003). Beneath the Tanzania Craton, our modeled lithosphere is slightly thinner than that beneath other African cratons but still shows a thick lithospheric keel of 140 to 160 km, similarly to the FB2011 and PMK2013 models. Our results also support the findings of a Rayleigh wave tomography study by Weeraratne et al. (2003), who imaged the LAB beneath the craton at a depth of 150 ± 20 km, demonstrating the stability of the Archean lithosphere in the presence of mantle upwelling. In southernmost Africa, our model agrees well with the thick lithosphere (> 160 km) imaged in the FB2011 and PMK2013 models (Fig. 11). A relative local lithospheric thickening is visible in all models, probably related to the collisional zone between the Kaapvaal and Zimbabwe cratons.

6.3 Crustal density and Moho depth

Using a linear, depth-dependent crustal density with a homogeneous average value throughout the continent results in a good fit with the available seismic data, but it does not necessarily satisfy the differences in crustal thickness for distinct tectonic domains. We observe local differences exceeding ±5 km between modeled and seismic estimates of Moho depth, which can be attributed to deviations from the initial crustal density profile. For instance, in the northwest Congo Craton, our crustal thickness values are ~8 km thinner compared with RF studies by Tokam et al. (2010), who image a significantly thick crust (~45 km). These authors also imaged a 23 km thick, high velocity lower crustal layer, which is >10 km thicker than beneath the Tanzania, Kaapvaal, and Zimbabwe cratons. The associated effect of the thick mafic layer can be related to an increase of 60 to 80 kg/m^3 on the bulk density of the crustal column. Increasing the average crustal density to 2870 kg/m^3 in the Congo Craton would result in a modeled crustal thickness of ~45 km, in agreement with seismic estimates.

Likewise, changing the input crustal density within bounds of ±40 kg/m^3 enabled us to associate misfits in southernmost Africa with variations in the local density structure. These variations can be related to magmatic events, which might have added high-density rocks to the crust (e.g., Namaqua-Natal Belt and Bushveld Igneous Complex) and/or to sediment accumulations that might have lowered the

bulk crustal density (e.g., in the Witwatersrand Basin). The related maximum variations in crustal thickness were about ±4.2 km and resulted in a complete fit of modeled crustal thickness compared to seismic estimates from the SASE experiment. In summary, it is possible to fit the estimated crustal thickness from seismic experiments by locally changing the average crustal density within reasonable bounds. However, using our methodology to calculate the crustal thickness for those regions of Africa where seismic data is not available, which is the major strength of our approach, has the tradeoff of assuming a homogeneous crustal density value because possible lateral density variations are mostly unconstrained.

6.4 Uncompensated topography in the Afar plume region

The Afar plume region, including the surrounding plateaus, exhibits rough topography, comprising a >1000 km wide domal uplift, intersected by the ~80 km wide MER valley, with highly uplifted rift flanks (>2000 m). The MER is surrounded by the elevated Ethiopian and Somalian plateaus (~1500 m) as well as a low relief (<500 m) zone to the north, in the Afar Depression. Further south, the effect of the plume extends to the Eastern Rift and the Kenya Dome. Our model shows overcalculated crustal thicknesses in this region, locally exceeding 15 km compared to available seismic observations (e.g., Maguire et al., 1994; Prodehl et al., 1997; Dugda et al., 2005; Wölbern et al., 2010; Figs. 5, 6, and 10). On average, the modeled crust is ~10 km thicker than estimates from RF studies by Dugda et al. (2005), who show thicknesses between 35 - 40 km in the Ethiopian Plateau, 30 - 35 km in the MER, and about 25 km in the Afar Depression. Upper mantle seismic tomography (Bastow et al., 2005; Benoit et al., 2006; Bastow et al., 2008) beneath the seismically and volcanically active MER shows a broad thermal upwelling or mantle plume from 75 km depth down to 400 km (Nyblade et al., 2000; Benoit et al., 2003; Nolet et al., 2003), which drives extension between the Nubian and Somalian plates. After plume impingement at ~30 Ma, a rapid lithospheric thinning occurred (Dugda et al., 2007; Gani et al., 2007), and broad Oligocene flood basalt volcanism affected the region, such that the thermally modified Pan-African lithosphere underlies huge portions of the Ethiopian Plateau and Afar Depression (Keranen et al., 2009). The Cenozoic interaction of mantle magmas with the crust (e.g., volcanism, dike intrusions, and underplating) would increase the average crustal density and the

calculated crustal thickness in the plateau, resulting in a larger misfit. Clearly, our modeling approach cannot conciliate the observed geoid and elevation with the measured crustal thickness in this region. As the thermal perturbation associated with the Afar plume might involve a dynamic component to the uplift in the plateau (e.g., Ebinger et al., 1989; Craig et al., 2011; Moucha and Forte, 2011; Faccenna et al., 2013), the overcalculated crustal thickness in our model could be explained by an offset in the input elevation data between the non-isostatic (dynamic) and the isostatic topography components.

In order to test if the model misfits in the Afar region can be explained by dynamic topography induced by sub-lithospheric buoyancy forces (e.g., Cazenave et al., 1989; Hager and Richards, 1989; Ricard et al., 1993), we tested the effect of the non-isostatic (dynamic) component of elevation on the calculated crustal thickness using a simplified setup. First, we assume a single plume, as suggested by various authors (Manighetti et al., 1997; Ebinger and Sleep, 1998; George et al., 1998; Gurnis et al., 2000; King and Ritsema, 2000; Davis and Slack, 2002), with a radius of r=1000 km, which is consistent with tomographic (Ritsema et al., 1999; Zhao, 2001; Ni et al., 2002) and mantle He isotope studies (Franz et al., 1999; Pik et al., 2006). The plume is centered at 42ºE, 11ºN near Lake Aheb in Afar, as indicated by structural, magnetic, and geochemical data (Schilling, 1973; Rooney et al., 2011). Second, we plot the observed crustal thickness from RF analysis by Dugda et al. (2005) and the EAGLE DSS survey by Maguire et al. (2006) against our calculated values (Fig. 12). This plot shows that, on average, the modeled crustal thickness exceeds the measured values by 9.81 km (y-intercept value in the regression line in Fig. 12). The isostatic contribution to elevation due to crustal thickness variations is:

$$\delta\varepsilon = \frac{(\rho_m - \rho_c)}{\rho_\epsilon}\delta h_c$$

where ρ_m, ρ_c, and ρ_ε are the densities of the mantle (3300 kg/m^3), crust (2790 kg/m^3), and topography (2670 kg/m^3), respectively, and δ_ε and δh_c are the variations of elevation and crustal thickness, respectively. Therefore, with the above considered densities, the topography associated with a change of 9.81 km in crustal thickness is 1874 m, which is the average residual topography relative to our model in the Afar region. Finally, we have assumed that the dynamic contribution (ε_r) to topography is

close to our inferred residual topography, and that it is a function of the radial distance *d* from the plume center, such that ε_r = 1800 m for 0 ≤ *d* ≤ 500 km and decreases linearly to zero, being $\varepsilon_r = 2 \times 1800 (1 - d/r)$ for 1000 ≥ *d* > 500 km. The so estimated dynamic contribution is then subtracted from the filtered ETOPO1 elevation corresponding to the location of each considered seismic station (Dugda et al., 2005; Maguire et al., 2006) and is used as the input data to recalculate the crustal thickness with our applied method.

Figure 13 shows the observed versus calculated crustal thicknesses for a combination of appropriate corrected elevations (-1600 to 1200 m), determined as described above, and for the corresponding geoid anomalies (2-7 m) in the Afar plume region, using a range of average crustal densities from 2790 to 2850 kg/m^3. After topography correction, the majority of the data fall inside the area of possible thickness solutions when the uncertainties associated with seismic experiments is also considered. It is worth noting that an increase in the average crustal density, probably related to magmatic processes, allows for a fit of about 71% of the observed crustal thickness values (Fig. 13). The resulting lithospheric thickness after corrections is reduced by ~60 km on average, thus also better fitting the tomography estimates.

Gravity, admittance, and river profile modeling (Roberts and White, 2010; Jones et al., 2012) suggest a maximum surface uplift of modern African swells from 800 to 2000 m. However, smaller peak amplitudes of dynamic topography (~700 m) are predicted in the EARS from mantle flow calculations based on subduction history (Lithgow-Bertelloni and Silver, 1998), and are estimated to be between 400 and 1200 m, based on mantle convection modeled backwards in time (Moucha and Forte, 2011). The positive signal in the Ethiopian dome has also been well established by regional investigations that show amplitudes up to 1000-1500 m (e.g., Faccenna et al., 2013; Gvirtzman et al., 2016). On the other hand, Molnar et al. (2015) proposed that mantle flow calculations tend to overestimate dynamic topography and therefore, our estimated non-isostatic topography of 1800 m must be considered as an upper bound.

7. Conclusions

We have constructed new maps of crustal and lithospheric thickness for continental Africa based on joint modeling of elevation and geoid data, combined with thermal analysis under the assumptions of local isostasy and thermal steady-state conditions. Our results are constrained by existing crustal thickness estimates from seismic experiments and from LAB depth estimations from tomography models. The integration of independent datasets sensitive to the density structure of the lithosphere into a coherent model has allowed us to image variations in both the crust and the lithospheric mantle structure offering a better confidence and resolution than previous studies.

We have compared our crustal thickness model with a comprehensive compilation of seismic estimates, which includes a total of 551 data locations, being the largest dataset used to benchmark data-driven crustal thickness maps. The compiled seismic data is unevenly distributed over four regions covering 20% of Africa. We find that the comparison between our calculated values with those from seismic estimates shows a similar accuracy as the CRUST1.0 model and considerably better fit with point observations than alternative gravity-derived models (e.g., Tedla2011 and Tugume2013 models), when the Afar region is excluded. The control on the quality of modeled crustal structure in those areas where seismic estimates are available encourages us to extrapolate our results to large regions of Africa where no seismic data exist (~80% of Africa) allowing us for a more confident image of its present-day crustal and lithospheric mantle structure.

From the presented work, we can draw the following concluding remarks:

- We have improved the applied methodology by defining a reference column at sea level to calculate the optimal average crustal density and geoid level, resulting in $\overline{\rho}_c$ = 2790 kg/m^3, N_0 = 6168 m, and a fit of 76.3% compared to available seismic observations, when the Afar plume region is excluded. The reference column has a crustal thickness of Z_c = 32.16 km and a total lithospheric thickness of Z_L = 153 km.

- Our calculated crustal thickness values across Africa are in overall good agreement with seismic estimates. Our final crustal model has a RMSE of 6.4

km and a fit of 61.0% relative to the whole compiled seismic dataset, showing the best minimum RMSE (4.3 km) and a maximum fit (76.3%) compared to other global and continental models, after excluding the Afar plume region.

- The crustal model depicts a bimodal distribution, with a clear north-south division and with distinct crustal structure and thicker cratonic crust in southern Africa (38-44 km) compared to northern Africa (33-39 km). The most striking feature is the crustal thinning (28-34 km) along the Mesozoic West African Rift separating the western and eastern regions of northern Africa. Overall, thick crust (37-48 km) is related to Archean cratons and shields as well as Proterozoic belts, whereas thin crust (28-30 km) is found along the Atlantic coastal zone and regions affected by the Mesozoic WCARS and the Cenozoic EARS extension.

- The calculated lithospheric thickness shows a large spatial variability, ranging from 90 to 230 km. Though the regional patterns of crust and lithospheric thickness share similarities, major differences are delineated in the Atlas region (northeast Morocco), where the crust is relatively thick compared to the lithospheric mantle; along the Mesozoic West African Rift, where the crust is relatively thin compared to the lithospheric mantle; and beneath the intracratonic basins (e.g., Congo Basin and Taoudeni Basin), where the maximum LAB depths exceeding 200 km are found.

- Comparing our crustal model with other existing models shows differences along the western and southern edges of the WAC, and along the West African Rift, where our model predicts large-scale crustal thinning instead of relative thickening. Our lithospheric model shows an overall similar pattern to that seen in tomography models, especially in Archean and Proterozoic regions (WAC, north WAMZ, Congo Basin, and Kaapvaal and Zimbabwe cratons).

- Density variations of ±60 kg/m^3 relative to the initial value of 2790 kg/m^3 result in minor crustal thickness changes of ±2 km for most parts of the African continent and up to ±5 km in the MER as well as in the Taoudeni, Congo, and Kalahari basins, allowing for a better fit with available seismic data. The

related differences in LAB depth were ±5 km, with maximum changes in the aforementioned regions of ±15 km.

- The sublithopsheric mantle flow associated with the Afar plume may involve a dynamic component to the topography in that region. The calculated crustal thickness in our model, that on average exceeds 9.8 km compared to seismic observations, can be corrected by applying a reduction in the elevation at seismic stations locations within a radius of 500 km from the center of the plume of ~1800 m. After corrections, the resulting LAB depth is reduced by ~60 km.

Acknowledgments

The project and the author J. Globig were funded by the European Commission grant Marie Curie Actions (264517-TOPOMOD-FP7-PEOPLE-2010-ITN). We are indebted to two anonymous reviewers who largely improved the first version of the manuscript through their comments and suggestions. The data for this paper are available by contacting the corresponding author at mfernandez@ictja.csic.es.

Figure Captions

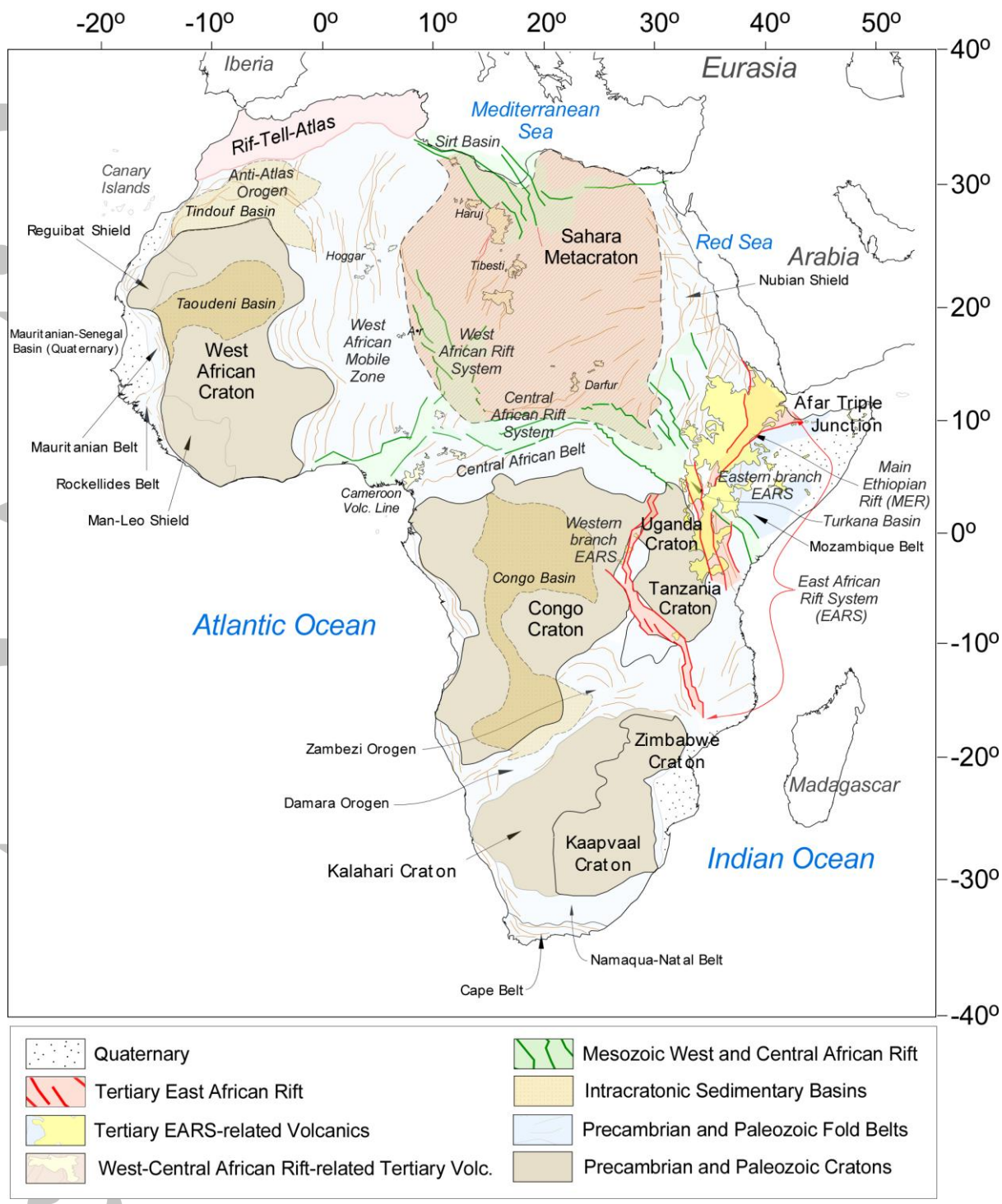

Figure 1. Simplified tectonic map of Africa, based on Milesi et al. (2010), showing the location and extent of the Archean Cratons, intracratonic basins, and the surrounding Precambrian and Paleozoic fold belts, which were affected by rifting processes during Mesozoic and Cenozoic times and by Cenozoic volcanism.

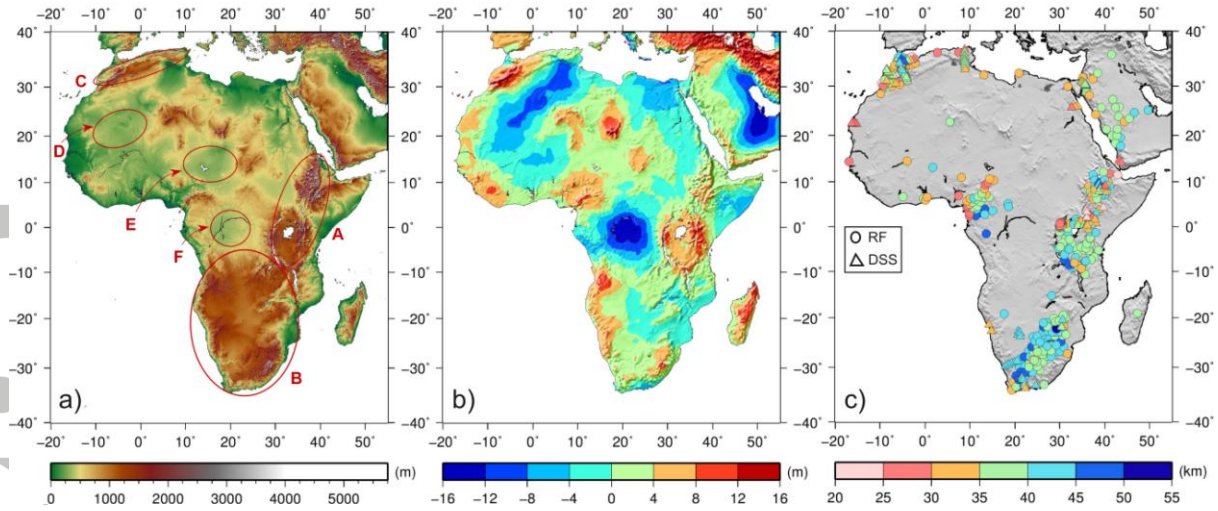

Figure 2. Geophysical data: a) Elevation map from the ETOPO1 global model (Amante and Eakins, 2009) after removing wavelengths <100 km. Red circles and labels highlight areas discussed in section 3.1. A-East African and Ethiopian Plateaus, B-Southern African Plateau, C-Rif-Tell-Atlas orogenic system, D-Taoudeni Basin, E-Chad Basin, F- Congo Basin.; b) Geoid anomaly map from the EGM2008 global model (Pavlis et al., 2012) after removing spherical harmonics up to degree and order of 10; c) Seismic estimates of crustal thickness from controlled-source seismic experiments and receiver function studies (see Table 2 for details).

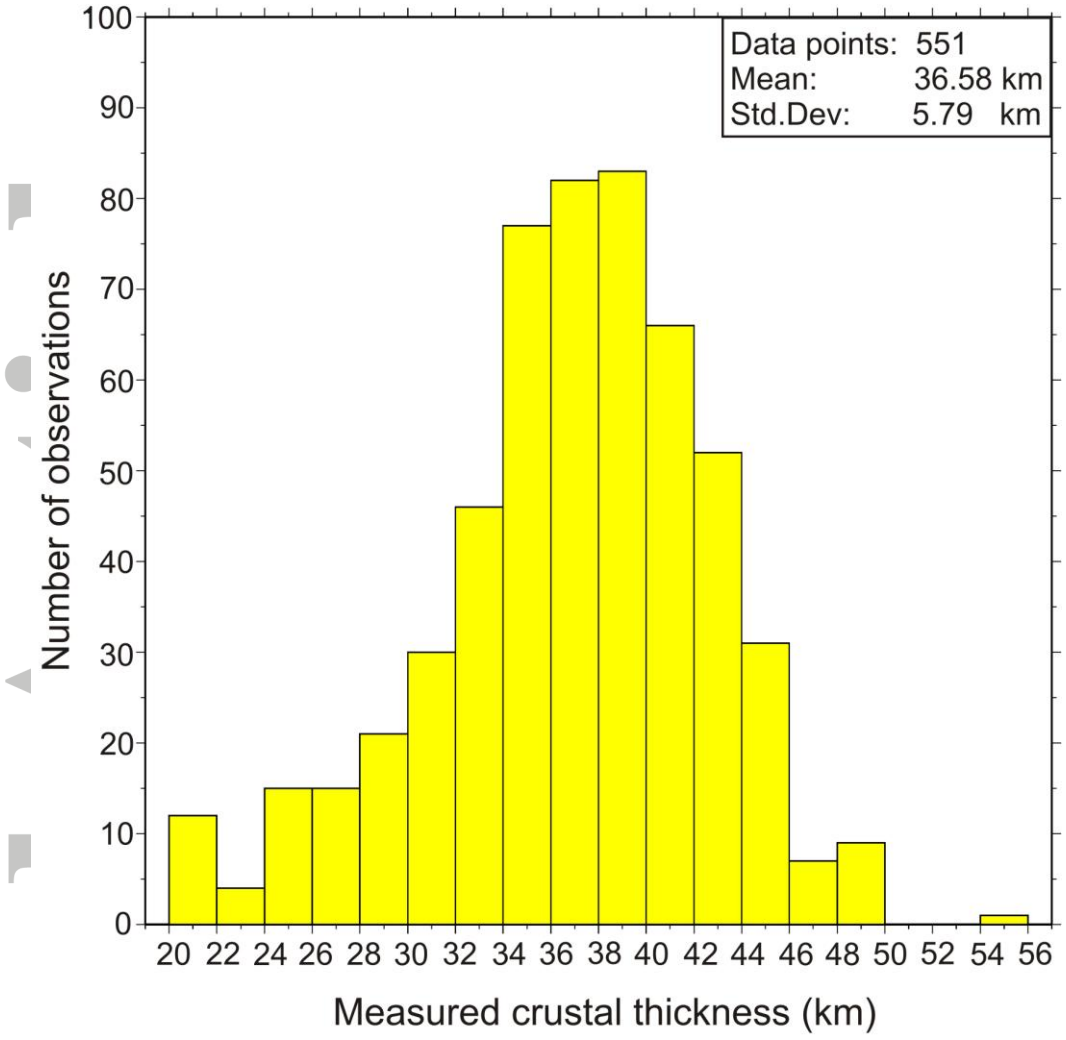

Figure 3. Histogram of estimated crustal thickness beneath Africa and Arabia from seismic experiments. See Figure 2c for station locations.

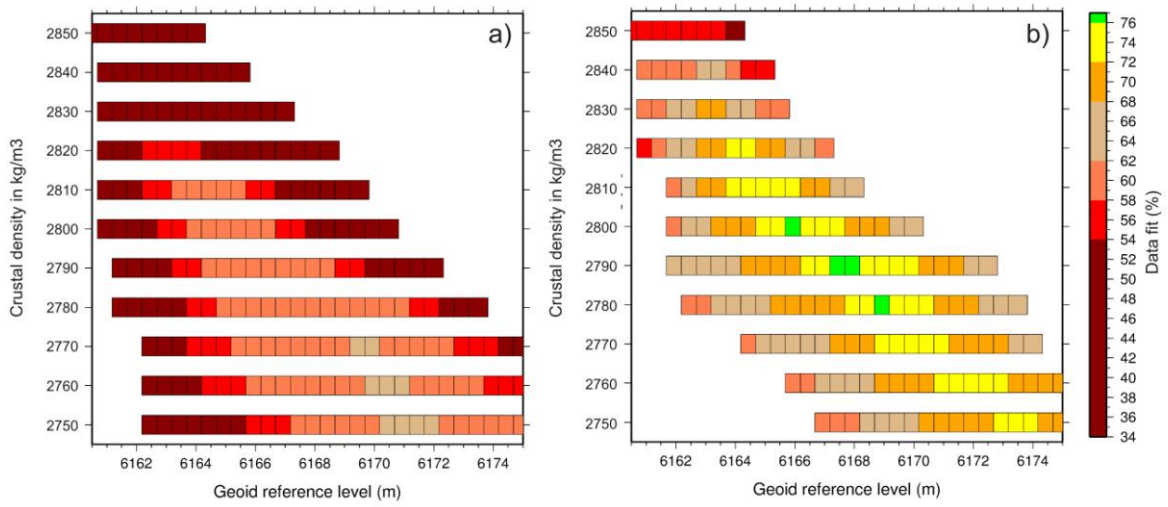

Figure 4. Degree of fit (in percent) between the calculated and observed crustal thickness for different reference columns determined by the average crustal density and geoid reference level values represented by individual boxes. a) Fit obtained considering all available seismic data in Africa and Arabia; b) Fit obtained considering all available seismic data in Africa but excluding the Afar plume region. Misfits are calculated considering uncertainties in the seismic estimates (±4 km for DSS and ±5 km for RF experiments).

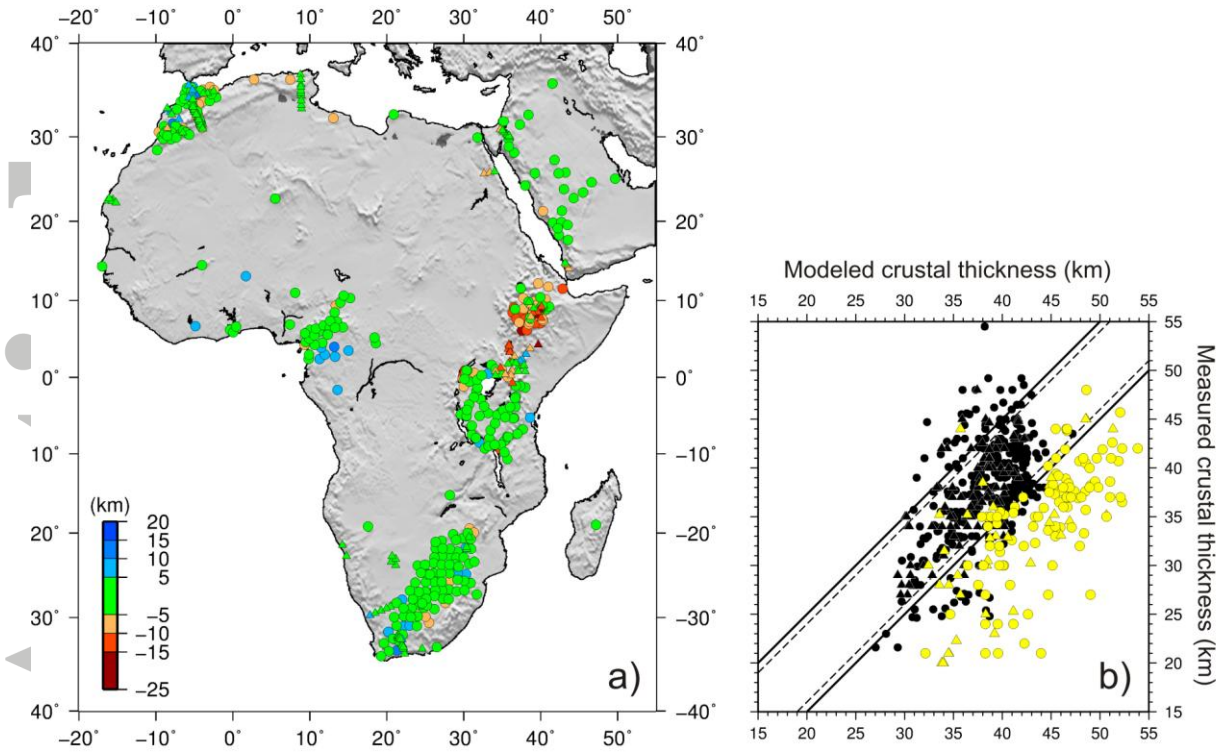

Figure 5. a) Difference between observed and calculated crustal thickness at each seismic station (see color scale). Triangles denote DSS experiments and circles from RF analyses. b) Scatterplot showing observed versus calculated crustal thickness. Black solid (±5 km) and dashed lines (±4 km) denote uncertainties related to seismic estimates. Colored symbols: yellow refers to the Afar plume region and black refers to the rest of Africa.

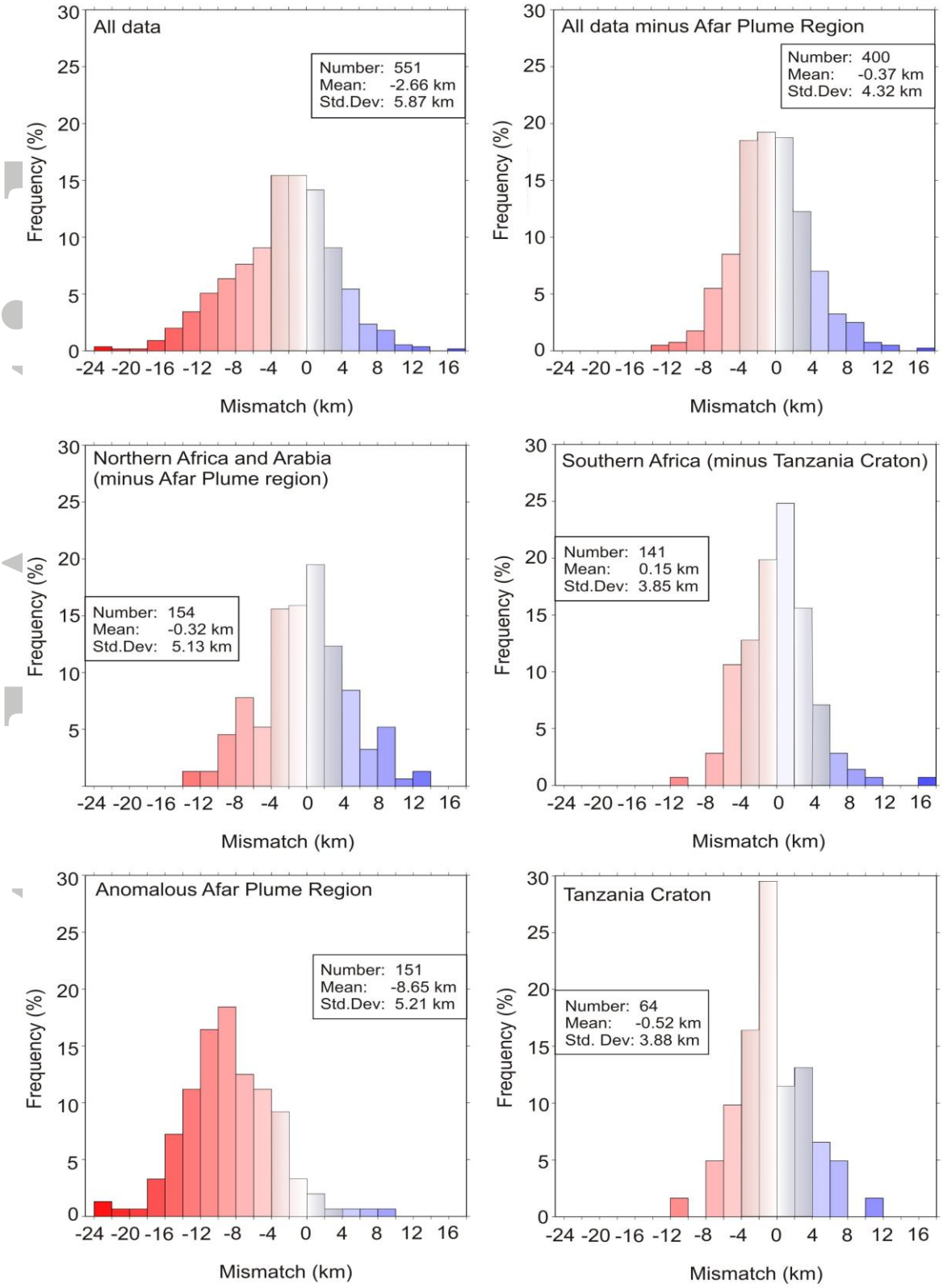

Figure 6. Histograms showing the mismatch between the observed and calculated crustal thickness estimates for the whole African dataset and for the different regions where seismic data are available. A positive/negative mean mismatch indicates average under/over calculated crustal thickness, respectively.

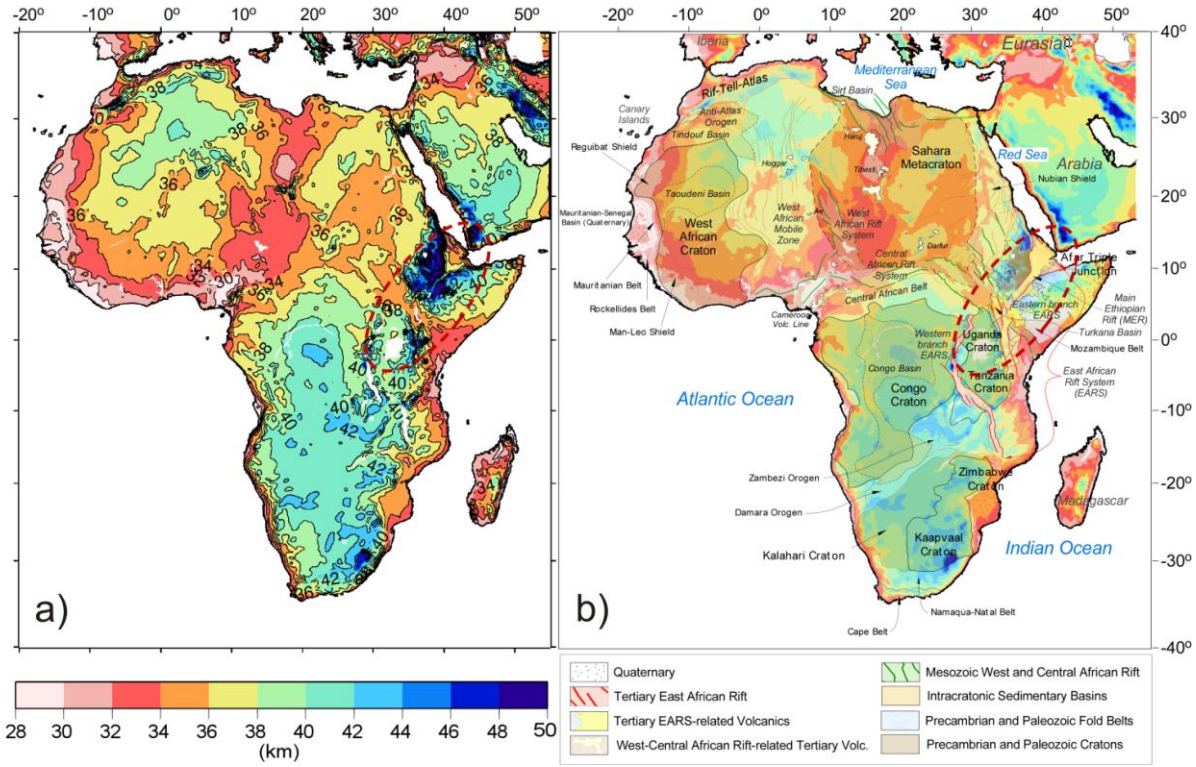

Figure 7. a) Calculated crustal thickness map with isolines every 2 km. b) Calculated crustal thickness map, superimposed on the structural map (Fig. 1) with the main tectonic units. Encircled area denotes the Afar plume region, where the crustal thickness is overcalculated because the assumptions of our approach are not fulfilled.

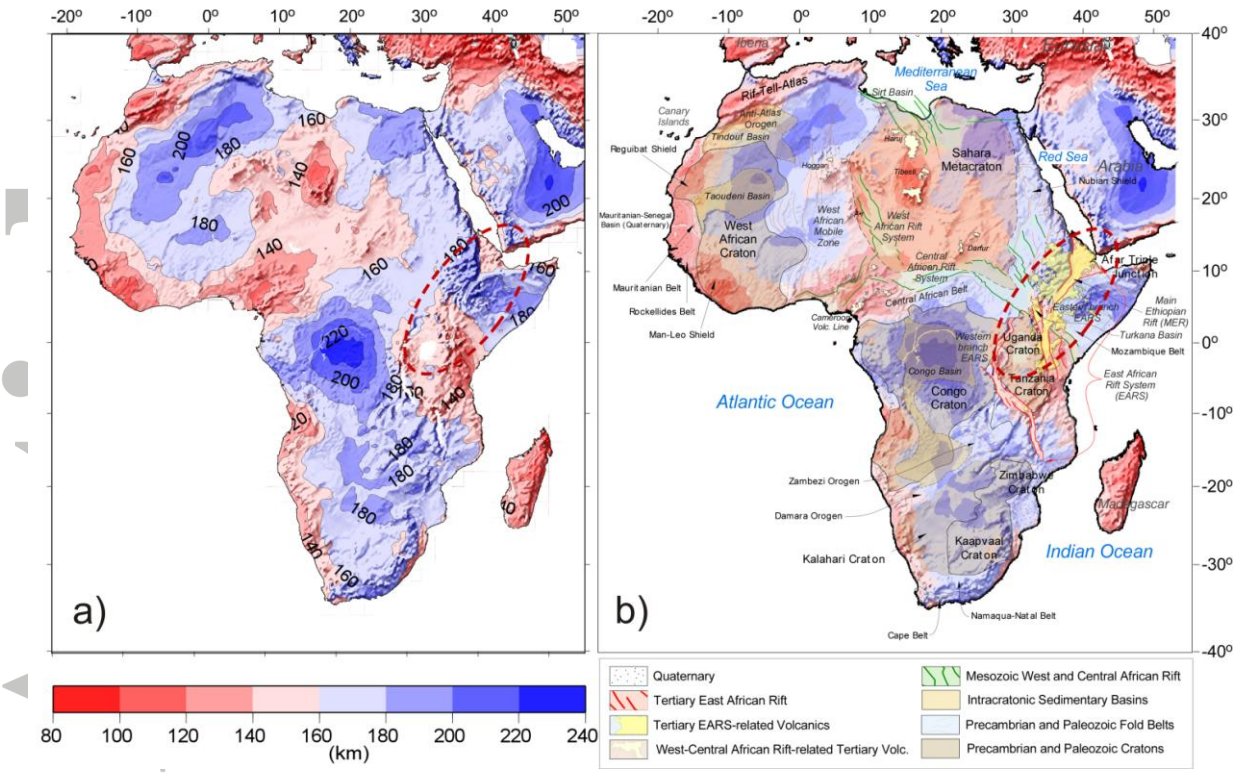

Figure 8. a) Calculated lithospheric thickness map with isolines every 20 km b) Calculated lithospheric thickness map superimposed on the structural map (Fig. 1) with the main tectonic units. Encircled area denotes the Afar plume region, where the lithospheric thickness is overcalculated because the assumptions of our approach are not fulfilled.

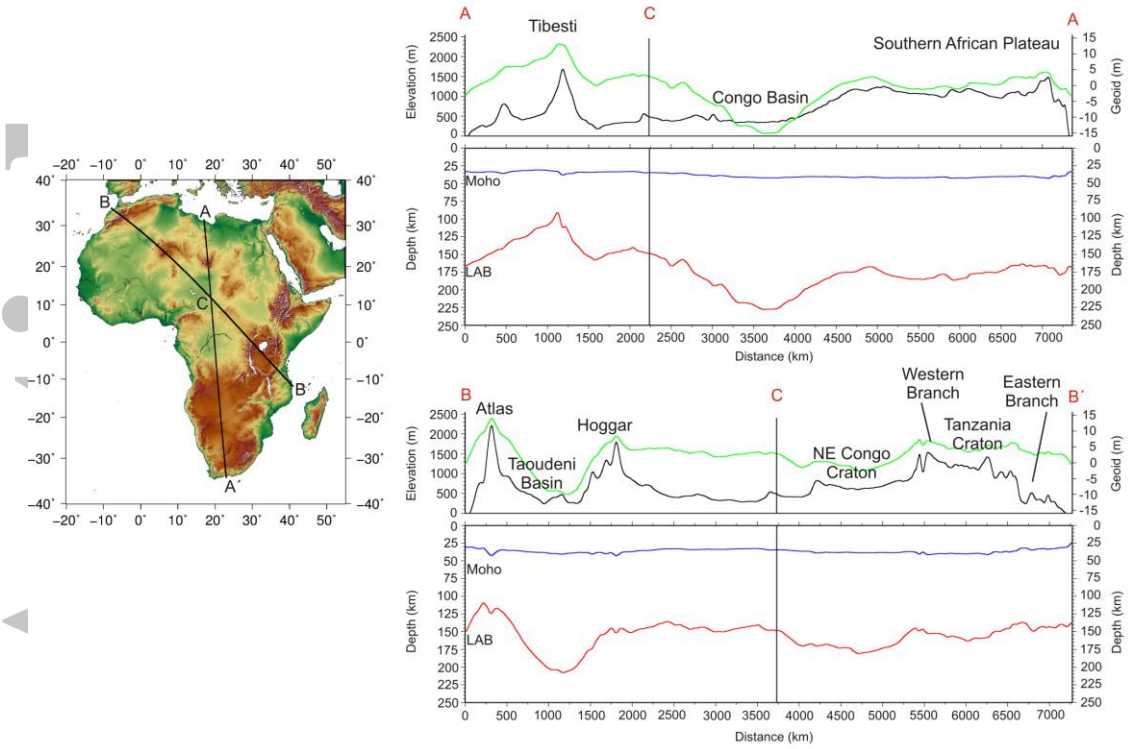

Figure 9. Lithospheric cross-sections across the Africa continent, showing the observed elevation (black line) and geoid height (green line) in the upper panels of each profile, and the calculated crustal (blue line) and lithospheric (red line) thickness in the lower panels of each profile. Different thickness ratios of crust and lithospheric mantle characterize the Tibesti and Hoggar hotspots and the Atlas Mountains, the Congo and Taoudeni intracratonic basins, and the cratonic domains of the Congo, Tanzania, and southern African Plateau.

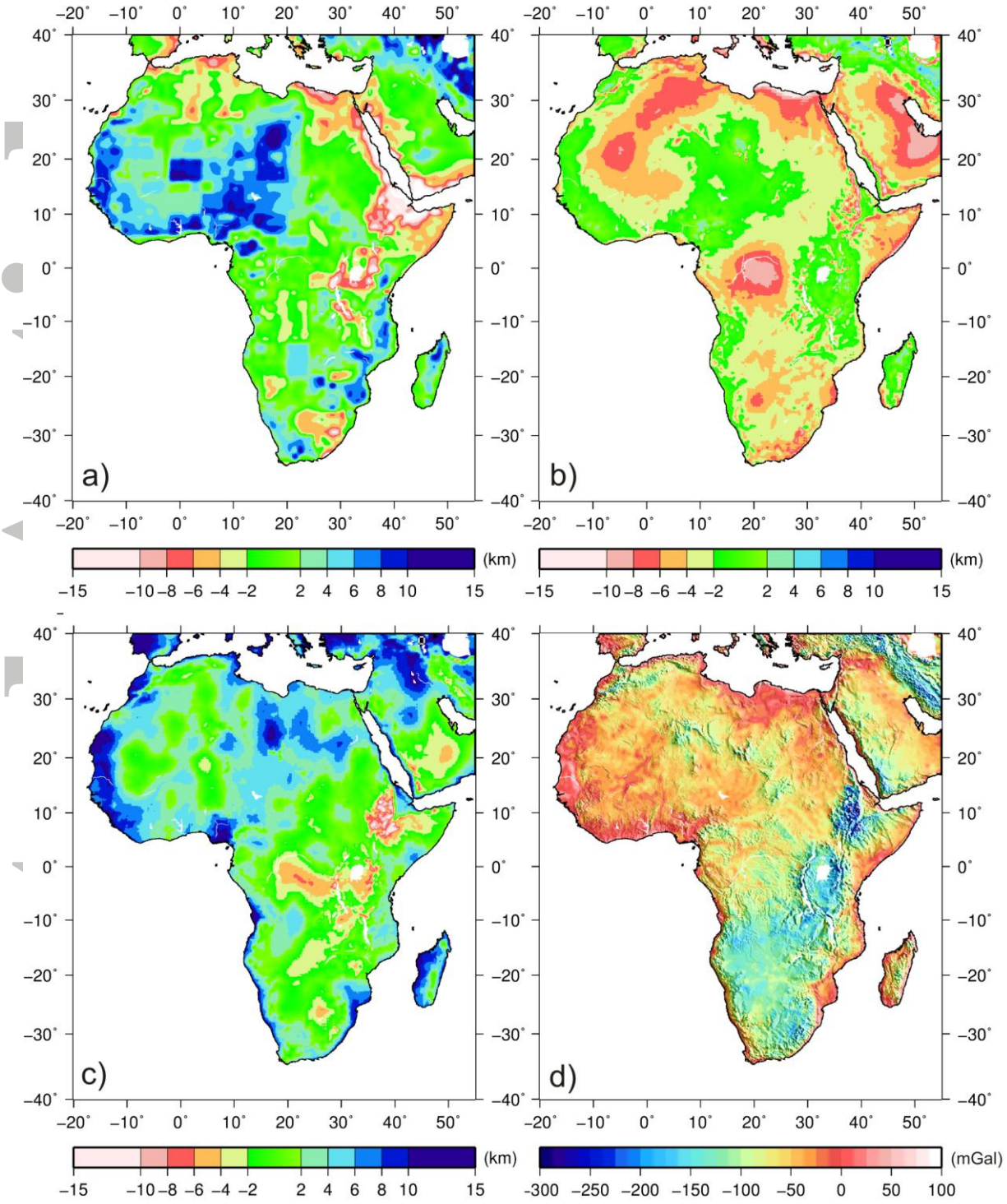

Figure 10. Comparison between global and regional crustal models and our model and gravity map of Africa. Differences are plotted as subtracted grids with respect to crustal thickness calculated in this study. a) CRUST1.0 (Laske et al., 2013); b) Tugume2013 (Tugume et al., 2013); c) Tedla2011 (Tedla et al., 2011); d) Bouguer anomaly map (Pérez-Gussinyé et al., 2009).

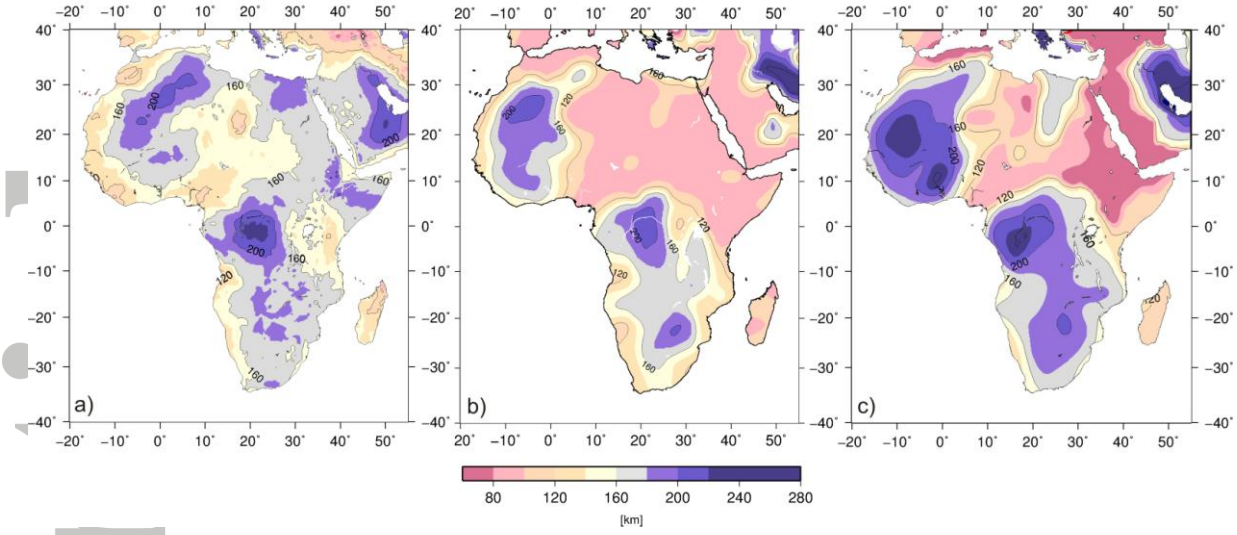

Figure 11. Lithospheric thickness maps of Africa. a) our model; b) global PMK2013 model (Priestley and McKenzie, 2013); c) continental FB2011 model (Fishwick and Bastow, 2011). The color scale has been adapted to facilitate the comparison with FB2011.

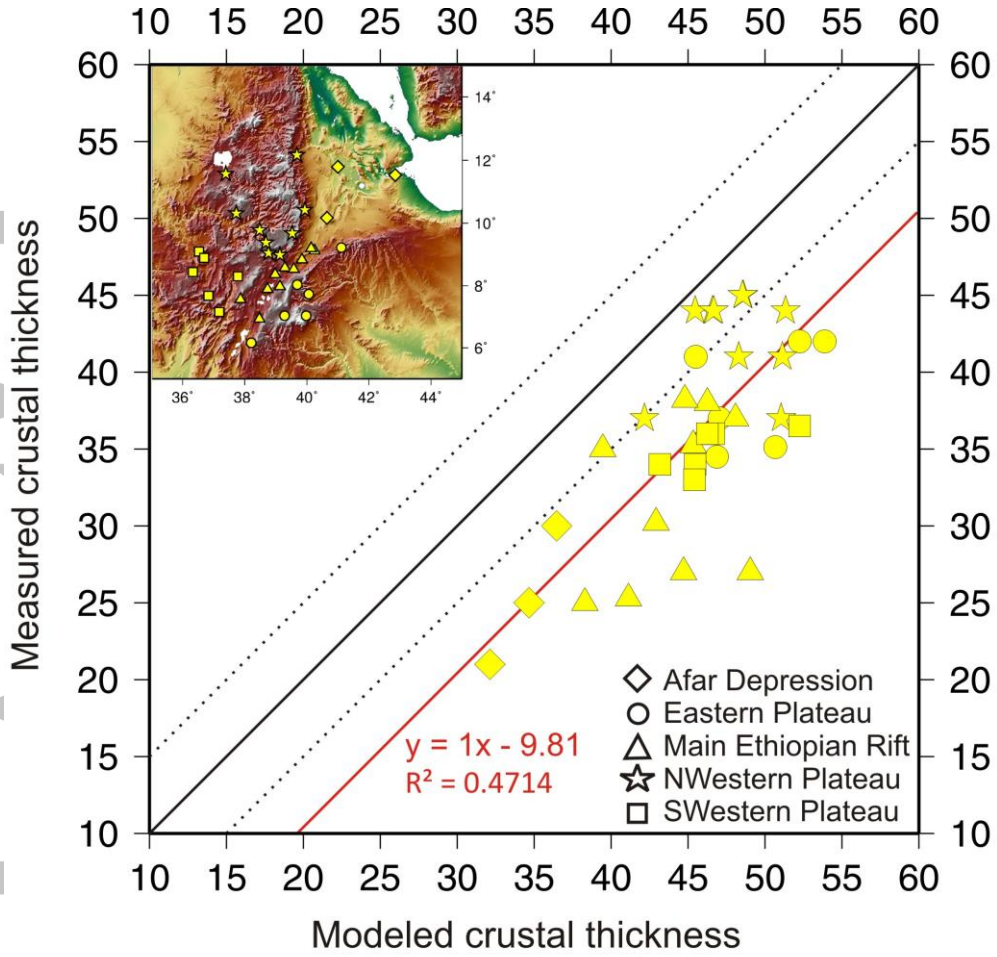

Figure 12. Scatterplot of observed (Dugda et al., 2005; Maguire et al., 2006) versus calculated crustal thickness (km) beneath the Ethiopian Plateau and the Afar depression (see inset for location). Solid black line denotes perfect agreement between observed and calculated values and dashed lines denote the associated uncertainties (±5 km). Red solid line corresponds to the regression line parallel to the 1:1 line, showing a shift of -9.81 km.

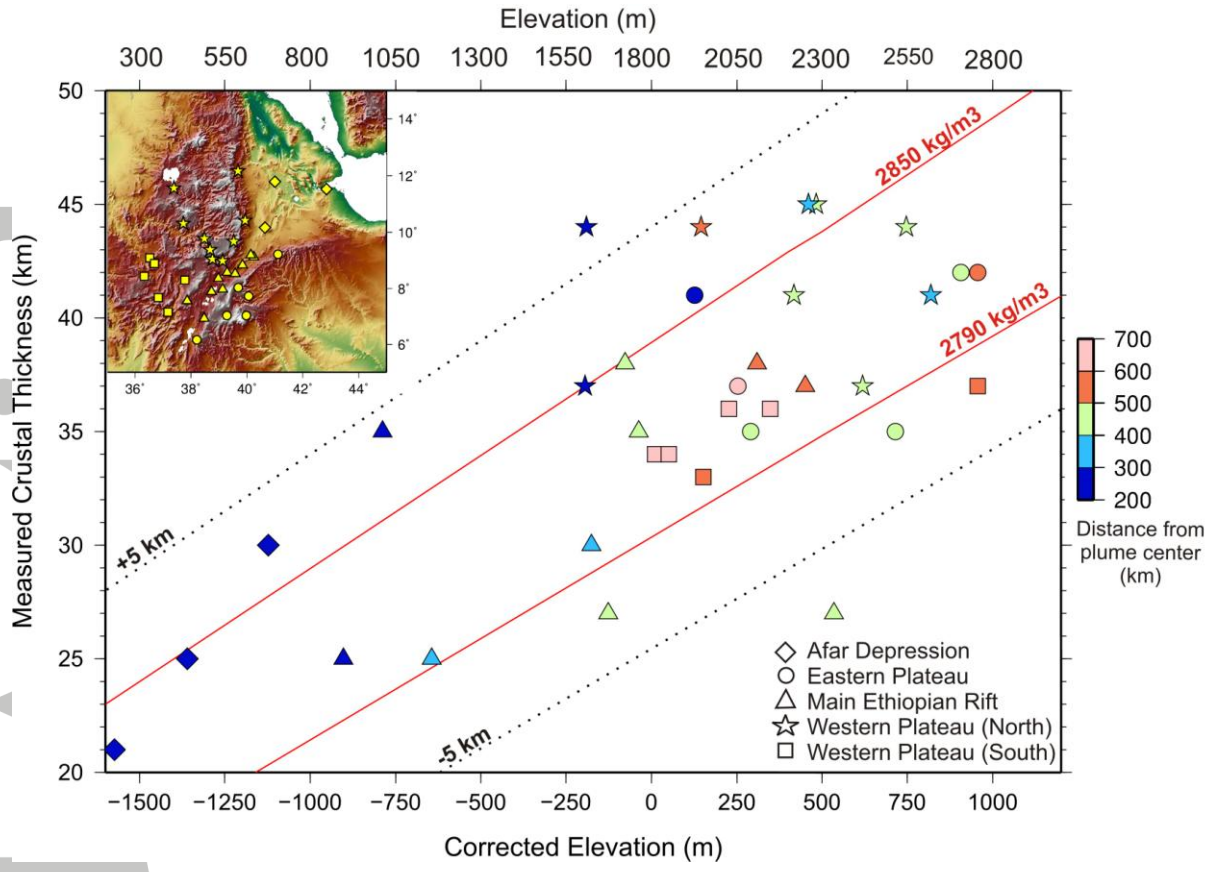

Figure 13. Crustal thickness from seismic experiments (Dugda et al., 2005; Maguire et al., 2006) plotted against corrected elevation from non-isostatic contribution to topography. Symbols denote the location of stations (see inset), and colors denote the distance to the center of the Afar plume. Topography correction is 1800 m for distances ≤500 km to the center of the plume and decreases linearly until vanishing at 1000 km distance. Red lines denote the range of average crustal densities considered in calculations and dashed lines denote the associated uncertainties (±5 km).

Tables

Table 1. Overview of previous global and continental crustal models, the applied method, and their corresponding resolution.

Model	Coverage	Method	Resolution	Reference
GMCT	Global	Seismic data compilation	2º	Soler et al. (1982)
M84C	Global	Seismic waveform inversion	8º	Woodhouse & Dziewonski (1984)
CM91	Global	Seismic data compilation	2º	Cadek & Martinec (1991)
3SMAC	Global	3D seismological model	2º	Nataf and Ricard (1996)
CRUST5.1	Global	Statistical inference based on seismic studies	5º	Mooney et al. (1998)
CRUST2.0	Global	Statistical inference based on seismic studies	2º	Bassin et al. (2000)
CUB2	Global	Surface wave inversion	2º	Schapiro & Ritzwoller (2002)
MDM	Global	Surface wave inversion	2º	Meier et al. (2007)
Pasyanos07	Continental	Surface wave analysis	1º	Pasyanos & Nyblade (2007)
SSLIP	Global	SS waveform stacks	10º	Rychert & Shearer (2010)
Tedla2011	Continental	Gravity, 3-D Euler deconvolution	0.225º	Tedla et al. (2011)
Tugume13	Continental	Gravity, Parker–Oldenburg iterative inversion	0.25º	Tugume_et al. (2013)
Gemma	Global	Combined gravity and seismic model	0.5º	Reguzzoni et al. (2013)
VMM	Global	Isostatic model	1º	Bagherbandi et al. (2013)
CRUST1.0	Global	Statistical inference based on seismic studies	1º	Laske et al. (2013)
DMM1	Global	Combined gravity and seismic model	2º	Hamayun (2014)

Table 2. Crustal thickness estimates for distinct tectonic terrains in Africa from a) DSS and b) RF studies.

a) Deep Seismic Sounding (DSS)		**b) Receiver Functions (RF)**	
Region	**Moho depth (km)**	**Region**	**Moho depth (km)**
		Northern Africa	
Rif	29 - 42[d]	Rif	21.6 - 44.4[1,3]
Tell (E)	29 - 37[e,f]	Atlas	23 - 44.7[1,2,14,15,16]
Atlas	33 - 41[a,b,c]	Meseta	30.7 - 37.6[1]
Meseta	~30[c]	Lybian Margin	~27[3]
Saharan Platform	~35[e]	Algerian Margin	30 - 31[3]
Morocco Margin (NW)	34 - 35[x]	Hoggar	~38[2]
Morocco Margin (SW)	27 - 29[y]	Egypt	32 - 33[2,3]
Red Sea	29 - 32[m]	Mauritanian Belt	~26.3[4]
Dead Sea Transform	29 - 38[n,o,p]	West African Craton	41 - 42.6[2,4,17]
Turkana Depression	20 - 21[l]	Afar Depression	15 - 30[6,7]
Afar Depression	~15[h]	Main Ethiopian Rift	27 - 38[6]
Main Ethiopian Rift	25 - 45[g]	Ethiopian Plateau	34 - 44[6]
		Cameroon Volcanic Line	25.5 - 40.5[5]
		Southern Africa	
Zimbabwe Craton	~40[q]	Zimbabwe Craton	35 - 50.5[10,11]
Limpopo Belt	35 - 37[q,r]	Limpopo Belt	39.5 - 46[10]
Namaqua-Natal Belt	40 - 45[s,t,v,w]	Namaqua-Natal Belt	30 - 49[10,12]
Cape Fold Belt	39.5 - 42[u,v]	Kenya Rift	34 - 44[6]
Namibian Margin	28 - 33[β]	Albertine Rift	24 - 38[8]
South African Margin (W)	~34[z]	Mozambique Belt	38 - 40[6]
South African Margin (S)	31 - 36.5[s,v]	Ruwenzory Belt	21 - 28[8]
		Kibaran Belt	36.7 - 44.4[9]
		Ubendian Belt	40 - 49.2[9]
		Usagaran Belt	32.3 - 39.6[9]
		Congo Craton	43 - 48[2,5]
		Tanzania Craton	37 - 44.4[9]
		Irumide Belt	~42.5[13]
		Kaapvaal Craton	33 - 53.5[10,13]
		Cape Fold Belt	33.5 - 48[10,12]
		Kheis Belt	35 - 48[10,11,12]

References: A) [a] Ayarza et al. (2014), [b] Wigger et al. (1992), [c] Makris et al. (1985), [d] Gil et al. (2014), [e] Buness et al. (2003), [f] Morelli and Nicolech (1990), [g] Maguire et al. (1994), [h] Prodehl et al. (1997), [l] Kahn et al. (1989), [j] Achauer et al. (1992), [k] Braile et al. (1994), [l] Gajewski et al. (1994), [m] Rihm et al. (1991), [n] Mechie et al. (2005), [o] Webb et al. (2004), [p] El-Isa et al. (1987), [q] Stuart and Zengeni (1987), [r] Durrrheim et al. (1992), [s] Lindeque et al. (2007), [t] Green and Durrheim (1990), [u] Parsiegla et al. (2009), [v] Stankiewicz et al. (2008), [w] Wright and Hall (1990), [x] Contrucci (2004), [y] Klingelhoefer et al. (2009), [z] Hirsch et al. (2009), [β] Bauer et al. (2000). B) [1]Mancilla et al. (2012), [2]Sandvol et al. (1998), [3]van der Meijde et al. (2003), [4]Kosarian (2006), [5]Tokam et al. (2010), [6]Dugda et al. (2005), [7]Hansen et al. (2009), [8]Wölbern et al. (2010), [9]Tugume (2011), [10]Youssof et al. (2013), [11]Nair et al. (2006), [12]Kagaswane et al. (2009), [13]Midzi and Oteemoeller (2001), [14]Miller and Becker (2013), [15]Spieker et al. (2014), [16]Cooper and Miller, [17]Di Leo et al. (2015).

Table 3. a) Statistical comparison of crustal thickness estimates from seismic experiments with published models for all of Africa and excluding the Afar region. Columns denote maximum and minimum differences, RMSE and degree of fit (in percent) considering uncertainties in the seismic estimates (±4 km for DSS and ±5 km for RF experiments) and considering the fit with our seismic Moho compilation applying the aforementioned fitting criteria.

Models	Max(km)	Min(km)	RMSE(km)	Fit(%)
	All data/Excl. Afar	All data/Excl. Afar	All data/Excl. Afar	All data/Excl. Afar
Our Model	16.3/16.3	-23.0/-13.9	6.4/4.3	61.0/76.3
CRUST1.0 (1)	18.5/18.5	-17.0/-15.7	5.3/5.0	69.9/74.5
Tedla (2)	12.7/12.7	-19.0/-16.4	6.4/5.9	57.9/59.3
Tugume (3)	18.9/18.9	-17.4/-11.3	6.1/5.3	56.6/64.0

References: (1) Laske et al. (2013); (2) Tedla et al. (2011); (3) Tugume et al. (2013).

Table 4: Model Input Parameter.

Parameter	Symbol	Value
Upper crustal density	ρc_{Top}	2630 kg/m^3
Lower crustal density	ρc_{Bottom}	2950 kg/m^3
Lithospheric mantle density	$\rho_m(T)$	3200*[1-3.2*10^{-5} (T-1350 ºC)]
Asthenosphere density	ρ_a	3200 kg/m^3
Sea water density	ρ_w	1030 kg/m^3
Compensation level depth	Z_{max}	300 km
Moho depth of the reference column	Z_{C_Ref}	32.16 km
LAB depth of the reference column	Z_{L_Ref}	153.1 km
Linear coefficient of thermal expansion	a	3.2 10^{-5}/K
Crustal surface heat production	H_S	0.5 µW/m^3
Crustal thermal conductivity	k_C	2.5 W/m K
Mantle thermal conductivity	k_M	3.2 W/m K
Surface temperature	T_S	0 ºC
Temperature at the LAB	T_a	1350 ºC

Table 5: Statistical comparison between referenced crustal models and our model (see Figure 10). The grid size in each comparison was adapted to the model with lower resolution. Columns denote maximum and minimum differences and RMSE.

Models	Max(km)	Min(km)	RMSE(km)
CRUST1.0[(1)] *minus* our model	16.1	-26.5	4.95
Tedla2011[(2)] *minus* our model	16.7	-15.8	4.45
Tugume2013[(3)] *minus* our model	10.5	-16.5	4.04
CRUST1.0[(1)] *minus* Tugume2013[(3)]	15.92	-18.89	5.99
CRUST1.0[(1)] *minus* Tedla2011[(2)]	11.55	-26.81	5.27
Tugume[(3)] *minus* Tedla[(2)]	5.72	-23.25	6.64

References: (1) Laske et al. (2013); (2) Tedla et al. (2011); (3) Tugume et al. (2013).

References

Abdelsalam, M., J. P. Liégeois, and R. J. Stern (2002), The Saharan metacraton, J. Afr. Earth Sci., 34, 119-136.

Abdelsalam, M. G., S.S. Gao, and J.P. Liégeois (2011), Upper mantle structure of the Saharan Metacraton, J. Afr. Earth Sci., 60, 328-336.

Achauer, U., P. K. Maguire, J. Mechie, W. V. Green, and the KRISP Working Group (1992), Some remarks on the structure and geodynamics of the Kenya rift, Tectonophysics, 213, 257-268.

Afonso, J. C., G. Ranalli, and M. Fernàndez (2005), Thermal expansivity and elastic properties of the lithospheric mantle: results from mineral physics of composites, Phys. Earth Planet. Int., 149, 279-306.

Al-Damegh, K., E. Sandvol, and M. Barazangi (2005), Crustal structure of the Arabian plate: new constraints from the analysis of teleseismic receiver functions, Earth Planet. Sci. Lett., 231, 177-196.

Amante, C., and B. W. Eakins (2009), ETOPO1 1 Arc-Minute Global Relief Model: Procedures, Data Sources and Analysis, NOAA Technical Memorandum NESDIS NGDC-24, 19.

Artemieva I. M., and W. D. Mooney (2001), Thermal thickness and evolution of Precambrian lithosphere: A global study, J. Geophys. Res., 106, 16, 387-16,414.

Artemieva I. M. (2006), Global 1°x1° thermal model TC1 for the continental lithosphere: implications for lithosphere secular evolution, Tectonophysics, 416, 245-277.

Ashwal L. D., and K. Burke (1989), African lithospheric structure, volcanism, and topography, Earth Planet. Sci. Lett., 96, 8-14.

Ayarza, P., R. Carbonell, and A. Teixell (2014), Crustal thickness and velocity structure across the Moroccan Atlas from long offset wide-angle reflection seismic data: The SIMA experiment, Geochem. Geophys. Geosyst., 15, 1698-1717.

Bagherbandi, M., R. Tenzer, L. E. Sjöberg, and P. Novák (2013), Improved global crustal thickness modeling based on the VMM isostatic model and non-isostatic gravity correction, J. Geodyn., 66, 25-37.

Bailey, D. K. (1992), Episodic alkaline igneous activity across Africa: Implications for the causes of continental break-up, in Magmatism and the causes of continental break-up, edited by B. C. Storey et al., Geol. Soc. Spec. Publ., 68, 91-98.

Bassin, C., G. Laske, and G. Masters (2000), The current limits of resolution for surface wave tomography in North America, Eos Trans. AGU 81, F897.

Bastow, I. D., G. W. Stuart, J. M. Kendall, and C. J. Ebinger (2005), Upper-mantle seismic structure in a region of incipient continental breakup: northern Ethiopian rift, Geophys. J. Int., 162, 479-493.

Bastow, I. D., A. A Nyblade, G. W. Stuart, T. O. Rooney, and M. H. Benoit (2008), Upper mantle seismic structure beneath the ethiopian hotspot: rifting at the edge of the African low velocity anomaly, Geochem. Geophys. Geosyst., 9(12), Q122022.

Batumike J. M., W. L. Griffin, and S. Y. O'Reilly (2009), Lithospheric mantle structure and the diamond potential of kimberlites in southern D. R. Congo, Lithos, 112, 166-176.

Bauer, K., S. Neben, B. Schreckenberger, R. Emmermann, K. Hinz, N. Fechner, K. Gohl, A. Schulze, R. B. Trumbull, and K. Weber (2000), Deep structure of the Namibia continental margin as derived from integrated geophysical studies, J. Geophys. Res., 105(B11), 25, 829-25,853, doi:10.1029/2000JB900227.

Begg, G., W. Griffin, L. Natapov, S. O'Reilly, S. Grand, C. O'Neill, J. Hronsky, Y. Djomani, C. Swain, T. Deen, and P. Bowden (2009), The lithospheric architecture of Africa: seismic tomography, mantle petrology, and tectonic evolution, Geosphere, 5, 23-50.

Behn M. D., C. P. Conrad, and P. Silver (2004), Detection of upper mantle flow associated with the African Superplume, Earth Planet. Sci. Lett., 224, 259-274.

Bell D., M. Grégoire, T. Grove, N. Chatterjee, R. Carlson, and P. Buseck (2005), Silica and volatile-element metasomatism of Archean mantle: a xenolith-scale

example from the Kaapvaal Craton, Contrib. Mineral. Petr., 150(3), 251-367.

Benoit, M. H., A. A. Nyblade, J. C. VanDecar, and H. Gurrola (2003), Upper mantle P-wave velocity structure and transition zone thickness beneath the Arabian Shield, Geophys. Res. Lett., 30(10), 1531, doi:10.1029/2002GL016436.

Benoit, M. H., A. A. Nyblade, and J. C. Van Decar (2006), Upper mantle P wave speed variations beneath Ethiopia and the origin of the Afar Hotspot, Geology 34, 329-332.

Bezada, M.J., E. D. Humphreys, D. R. Toomey, M. Harnafi, J. M. Davila, and J. Gallart (2013), Evidence for slab rollback in westernmost Mediterranean from improved upper mantle imaging, Spain, Earth Planet. Sci. Lett., 368, 51-60.

Black, R., and M. Girod (1970), Late Palaeozoic to Recent igneous activity in the West Africa and its relationship to basement structure, in African Magmatism and Tectonics, edited by T. N. Clifford and I. G. Gass, Oliver and Boyd, Edinburgh, 185-210.

Braile L. W, B. Wang, C. R. Daudt, G. R. Keller, and J. P. Patel (1994), Modeling the 2-D seismic velocity structure across the Kenya rift, Tectonophysics, 236, 251-269.

Buck, W. R. (1986), Small-scale convection induced by passive rifting: The cause for uplift of rift shoulders, Earth Planet. Sci. Lett., 77, 362-372.

Buiter, S. J. H., B. Steinberger, S. Medvedev, and J. Tetreault (2012), Could the mantle have caused subsidence of the Congo Basin?, Tectonophysics, 514-517, 62-80, doi:10.1016/j.tecto.2011.09.024.

Buness, H., P. Giese, C. Bobier, C. Eva, F. Merlanti, R. Pedone, and S. Mueller (1992), The EGT-85 seismic experiment in Tunisia - a reconnaissance of the deep structure, Tectonophysics, 207, 245-267.

Burke, K., and A. J. Whiteman (1973), Uplift, rifting and the break-up of Africa, in Implications of Continental Drift to the Earth, edited by D. H. Tarling, and S. K. Runcorn, Science, 2, 734-755.

Burke, K. (1996), The African plate, S. Afr. J. Geol., 99, 339-410.

Cadek, O., and Z. Martinec (1991), Spherical harmonic expansion of the Earth's crustal thickness up to degree and order 30, Stud. Geoph. Geod., 35, 151-165.

Camelbeeck, T., and M. D. Iranga (1996), Deep crustal earthquakes and active faults along the Rukwa trough, eastern Africa, Geophys. J. Int., 124, 612-630.

Cavaroc, V. V., G. Padgett, D. G. Stephens, W. H. Kanes, Boudda-Ahmed, and I. D. Wollen (1976), Late Paleozoic of the Tindouf Basin-North Africa, J. Sediment. Petrol., 46, 77-88.

Cazenave, A., A. Souriau, and K. Dominh (1989), Global coupling of Earth surface topography with hotspots, geoid and mantle heterogeneities, Nature, 340, 54-57.

Chesler, R. (2012), The Geochemistry and Geochronology of Tanzanian Kimberlites, School of Earth Sciences, The University of Melbourne, Melbourne.

Chevrot, S., and L. Zhao (2007), Multiscale finite-frequency Rayleigh wave tomography of the Kaapvaal craton, Geophys. J. Int., 169, 201-215.

Chorowicz, J. (2005), The East African Rift System, J. Afr. Earth Sci., 43, 379-410.

Conrad, C. P., and C. Lithgow-Bertelloni (2006), Influence of continental roots and asthenosphere on plate-mantle coupling, Geophys. Res. Lett., 33, L05312.

Contrucci, I., F. Klingelhoefer, J. Perrot, R. Bartolome, M. A. Gutscher, M. Sahabi, J. Malod, and J. P. Rehault (2004), The crustal structure of the NW Moroccan continental margin from wide-angle and reflection seismic data, Geophys. J. Int., 159, 117-128.

Cooper, C. M., and M. S. Miller (2014), Craton formation: Internal structure inherited from closing of the early oceans, Lithosphere, 6, 35-42.

Cornwell, D. G., P. K. H. Maguire, R. W. England, and G. W. Stuart (2010), Imaging detailed crustal structure and magmatic intrusion across the Ethiopian Rift using a dense linear broadband array, Geochem. Geophys. Geosyst.,11, Q0AB03.

Craig, T. J., J. A. Jackson, K. Priestley, and D. McKenzie (2011), Earthquake distribution patterns in Africa: their relationship to variations in lithospheric and geological structure, and their rheological implications, Geophys. J. Int., 185, 403-434, doi:10.1111/j.1365-246X.2011.04950.x.

Crosby, A. G., S. Fishwick, and N. White (2010), Structure and evolution of the intracratonic Congo Basin, Geochem. Geophys. Geosyst., 11, 6.

Davis, P. M., and P. D. Slack (2002), The uppermost mantle beneath the Kenya dome and relation to melting, rifting and uplift in East Africa, Geophys. Res. Lett., 29, 1117.

Deen, T., W. L. Griffin, G. Begg, S. Y. O'Reilly, and L. M. Natapov (2006), Thermal and compositional structure of the subcontinental lithospheric mantle: Derivation from shear-wave seismic tomography, Geochem. Geophys. Geosyst., 7, Q07003, doi:10.1029/2005GC001120. .

DESERT Group (2004), The crustal structure of the Dead Sea Transform, Geophys. J. Int., 156, 655-681.

deWit, M. J., C. Roering, R. J. Hart, R. A. Armstrong, C. E. J. deRonde, R. W. E. Green, M. Tredoux, E. Peberdy, and R. A. Hart (1992), Formation of an Archean continent, Nature, 357, 553-562.

Di Leo, J. F., J. Wookey, J. M. Kendall, and N. D. Selby (2015), Probing the edge of the West African Craton: a first seismic glimpse from Niger, Geophys. Res. Lett. 42, 1694-1700.

Dopp S. (1964), Preliminary note on a refracted P phase in the Western Rift Valley of Africa, J. Geophys. Res., 69, 3027-3031.

Doucouré, C. M., and M. J. De Wit, (2003), Old inherited origin for the present near-bimodal topography of Africa, J. Afr. Earth Sci., 36, 371-388.

Downey, N. J., and M. Gurnis (2009), Instantaneous dynamics of the cratonic Congo basin, J. Geophys. Res., 114, 6401, doi:10.1029/2008JB006066.

Dugda, M. T., A. A. Nyblade, J. Julia, C. A. Langston, C. A. Ammon, and S. Simiyu (2005), Crustal structure in Ethiopia and Kenya from receiver function analysis: implications for rift development in eastern Africa, J. Geophys. Res., 110, B01303, doi:10.1029/2004JB003065.

Dugda, M. T., A. A. Nyblade, and J. Julià (2007), Thin Lithosphere Beneath Ethiopia and Djibouti Revealed by a Joint Inversion of Rayleigh Wave Group Velocties and Receiver Functions, J. Geophys. Res., 112, B08305, doi:10.1029/2006JB004918.

Durrheim, R. J., W. H. Barker, and R. W. E. Green (1992), Seismic studies in the Limpopo belt, Precambrian Res., 55, 187-200.

Eaton, D. W., F. Darbyshire, R. L. Evans, H. Grütter, A. G. Jones and X., Yuan (2009), The elusive lithosphere-asthenosphere boundary (LAB) beneath cratons, Lithos, 109, 1-22.

Ebinger, C. J., T. Bechtel, D. Forsyth, and C. Bowin (1989), Effective elastic plate thickness beneath the East African and Afar plateau, and isostatic compensation for the uplifts, J. Geophys. Res., 94, 2893-2901.

Ebinger, C. J., and N. H. Sleep (1998), Cenozoic magmatism throughout east Africa resulting from impact of a single plume, Nature, 395, 788-791.

El-Isa, Z., J. Mechie, C. Prodehl, J. Makris, and R. Rihm (1987), A crustal structure study of Jordan derived from seismic refraction data, Tectonophysics, 138, 235-253.

England, P., and P. Molnar (1997), Active deformation of Asia: From kinematics to dynamics, Science, 278, 647-650.

Faccenna, C., C. Piromallo, A. Crespo-Blan, L. Jolivet, and F. Rossetti (2004), Lateral slab deformation and the origin of the western Mediterranean arcs, Tectonics, 23, TC1012.

Faccenna, C., T. W. Becker, L. Jolivet, and M. Keskin (2013), Mantle convection in the Middle East: reconciling Afar upwelling, Arabia indentation and Aegean trench

rollback, Earth Planet. Sci. Lett., 375, 254-269.

Fairhead, J. D., and C. V. Reeves (1977), Teleseismic delay times, Bouguer anomalies, and inferred thickness of the African lithosphere, Earth Planet. Sci. Lett., 36, 63-76.

Fairhead, J. D. (1986), Geophysical controls on sedimentation within the African rift systems, in Sedimentation in the African rifts, edited by L. Frostick et al., Geol. Soc. Spec. Publ., 25, 19-27.

Fairhead, J. D., and C. S. Okereke (1987), A regional gravity study of the West African rift system in Nigeria and Cameroon and its tectonic interpretation, Tectonophysics, 143, 141-159.

Fairhead, J. D. (1988), Mesozoic plate tectonic reconstructions of the Central-South Atlantic Ocean: the Role of the West and Central African Rift System, Tectonophysics, 155, 181-191.

Fairhead, J. D., and C. M. Green (1989), Controls on rifting in Africa and the regional tectonic model for the Nigeria and East Niger rift basins, in Rifting in Africa, edited by B. R. Rosendahl, Afr. Earth Sci. Spec. Publ., 8, 231-249.

Fernàndez, M., I. Marzán, A. Correia, and E. Ramalho (1998), Heat flow, heat production and lithospheric thermal regime in the Iberian Peninsula, Tectonophysics, 291, 29-53.

Fezaa, N., J. P. Liégeois, N. Abdallah, E. H. Cherfouh, B. De Waele, O. Bruguier, and O. Ouabadi (2010), Late Ediacaran geological evolution (575-555 Ma) of the Djanet Terrane, Eastern Hoggar, Algeria, evidence for a Murzukian intracontinental episode, Precambrian Res., 180, 299-327.

Fishwick, S. (2010), Surface wave tomography: Imaging of the lithosphere-asthenosphere boundary beneath central and southern Africa?, Lithos, 120, 63-73.

Fishwick, S., and I. D. Bastow (2011), Towards a better understanding of African topography, a review of passive-source seismic studies of the African crust and upper mantle, in The Formation and Evolution of Africa: A Synopsis of 3.8 Ga of Earth History, edited by D. J. J. Van Hinsbergen et al., Geol. Soc. Spec. Publ., 357, 343-371.

Forte, A. M., J. X. Mitrovica, R. Moucha, N. A. Simmons, and S. P. Grand (2007), Descent of the ancient Farallon slab drives localized mantle flow below the New Madrid seismic zone, Geophys. Res. Lett., 34, L04308.

Forte, A. M., S. Quéré, R. Moucha, N. A. Simmons, S. P. Grand, J. X. Mitrovica, and D. B. Rowley (2010), Joint seismic-geodynamic-mineral physical modelling of African geodynamics: a reconciliation of deep-mantle convection with surface geophysical constraints, Earth Planet. Sci. Lett., 295, 329-34.

Fouch, M. J., D. E. James, J. C. van Decar, S. van Der Lee (2004), Mantle seismic

structure beneath the Kaapvaal and Zimbabwe Cratons, S. Afr. J. Geol., 107, 33-44, doi:10.2113/107.1-2.33.

Franz, G., G. Steiner, F. Volker, D. Pudlo, and K. Hammerschmidt (1999), Plume-related alkaline magmatism in central Africa-the Meidob Hills (W Sudan), Chem. Geol., 157, 27-47.

Freybourger, M., J. B. Gaherty, and T. H. Jordan (2001), Structure of the Kaapvaal craton from surface waves, Geophys. Res. Lett., 28, 2489-2492.

Frizon de Lamotte, D., B. Saint Bezar, R. Bracene, and E. Mercier (2000), The two main steps of the Atlas building and Geodynamics of West Mediterranean, Tectonics, 19, 740-761.

Frizon de Lamotte, D., B. Fourdan, S. Leleu, F. Leparmentier, and P. Clarens (2015), Style of rifting and the stages of Pangea breakup, Tectonics, 34, 1009-1029.

Fullea, J., M. Fernàndez, H. Zeyen, and J. Vergés (2007), A rapid method to map the crustal and lithospheric thickness using elevation, geoid anomaly and thermal analysis. Application to the Gibraltar Arc System and adjacent zones, Tectonophysics, 430, 97-117.

Furman, T., J. Bryce, J. Karson, and A. Iotti (2004), East African Rift System (EARS) plume structure: insights from Quaternary Mafic Lavas of Turkana, Kenya, J. Petrol., 45, 1069-1088.

Gajewski, D., A. Schulte, D. Riaroh, and H, Thybo (1994), Deep seismic sounding in the Turkana depression, northern Kenya rift, in Crustal and Upper Mantle Structure of the Kenya Rift, edited by C. Prodeh et al., Tectonophysics, 236, 165-178.

Gani, N. D., M. R. Gani, and M. G. Abdelsalam (2007), Blue Nile incision on the Ethiopian Plateau: Pulsed plateau growth, Pliocene uplift, and hominin evolution, GSA Today, 17, 4-11.

Garcia-Castellanos, D., and A. Villaseñor (2011), Messinian salinity crisis regulated by competing tectonics and erosion at the Gibraltar Arc, Nature, 480, 359-363.

George, R., N. Rogers, and S. Kelley (1998), Earliest magmatism in Ethiopia: evidence for two mantle plumes in one flood basalt province, Geology, 26, 923-926.

Gil, A., J. Gallart, J. Diaz, R. Carbonell, M. Torne, A. Levander, and M. Harnafi (2014), Crustal structure beneath the Rif Cordillera, North Morocco, from the RIFSIS wide-angle reflection seismic experiment, Geochem. Geophys. Geosyst., 15, 4712-4733.

Grand, S. P., R. D. Van Der Hilst, and S. Widiyantroro (1997), Global seismic tomography: A snapshot of convection in the earth, GSA Today, 7, 1-7.

Green, R. W. E., and R. J. Durrheim (1990), A seismic refraction investigation of the Namaqualand Metamorphic Complex, South Africa, J. Geophys. Res., 95, doi:10.1029/89JB03582.

Gurnis, M., J. X. Mitrovica, J. Ritsema, and H. J. van Heijst (2000), Constraining mantle density structure using geological evidence of surface uplift rates: The case of the African superplume, Geochem. Geophys. Geosyst., 1, 7.

Gvirtzman, Z., C. Faccenna, and T. W. Becker (2016), Isostasy, flexure, and dynamic topography, Tectonophysics, doi:10.1016/j.tecto.2016.05.041.

Hager, B. H., R. W. Clayton, M. A. Richards, R. P. Comer, and A. M. Dziewonski (1985), Lower mantle heterogeneity, dynamic topography and the geoid, Nature, 313, 541-546.

Hager, B. H., and M. A. Richards (1989), Long-wavelength variations in Earth's geoid: physical models and dynamical implications, Phil. Trans. R. So. Lond. A, 328, 309-327.

Halliday, A. N., J. P. Davidson, P. Holden, C. Dewolf, D. C. Lee, and J. G. Fitton (1990), Trace-element fractionation in plumes and the origin of HIMU mantle beneath the Cameroon Line, Nature, 347, 523-528.

Hamayun (2014), Earth structure recovery from state-of-the art model of gravity field and additional geophysical information, PhD thesis, TU Delft.

Hamza, V. M., and F. P. Vieira (2012), Global distribution of the lithosphere-asthenosphere boundary: a new look, J. Geophys. Res. Solid Earth, 3(2), 199-212.

Hansen, S. E., A. A. Nyblade, J. Julia, P. H. G. M. Dirks, and R. J. Durrheim (2009), Upper-mantle low-velocity zone structure beneath the Kaapvaal craton from S-wave receiver functions, Geophys. J. Int., 178(2), 1021-1027.

Hansen, S., A. A. Nyblade, and M. Benoit (2012), Mantle structure beneath Africa and Arabia from adaptively parameterized P-wave tomography: Implications for the origin of Cenozoic Afro-Arabian tectonism, Earth Planet. Sci. Lett., 319-320, 23-34.

Hansen, S. E., and A. A. Nyblade (2013), The Deep Seismic Structure of the Ethiopia/Afar Hotspot and the African Superplume, Geol. J. Int., 194, 118-124.

Haxby, W. F., and D. L. Turcotte (1978), On isostatic geoid anomalies, J. Geophys. Res., 83(B11), 5473-5478, doi:10.1029/JB083iB11p05473.

Hilton, D. R., S. A. Halldórsson, P. H. Barry, T. P. Fischer, J. M. de Moor, C. J. Ramirez, F. Mangasini, and P. Scarsi (2011), Helium isotopes at Rungwe Volcanic Province, Tanzania, and the origin of East African Plateaux, Geophys. Res. Lett., 38, L21304.

Hirsch, K. K., K. Bauer, and M. Scheck-Wenderoth (2009), Deep structure of the

western South African passive margin Results of a combined approach of seismic, gravity and isostatic investigations, Tectonophysics, 470, 57-70.

Jaffal, M., F. Klingelhoefer, L. Matias, F. Teiseira, and M. Amrhar (2009), Crustal structure of the NW Moroccan margin from deep seismic data (SISMAR cruise), C. R. Geosci., 341, 495-503, doi:10.1016/j.crte.2009.04.003.

James, D. E., M. J. Fouch, J. C. VanDecar, S. van der Lee, and KAAPVAAL SEISMIC GROUP (2001), Tectospheric structure beneath southern Africa, Geophys. Res. Lett., 28, 2485-2488.

James, D. E., F. Niu, and J. Rokosky (2003), Crustal structure of the Kaapvaal Craton and its significance for early crustal evolution, Lithos, 71, 413-429.

Jarvis, G. T., and D. P. McKenzie (1980), Sedimentary basin formation with finite extension rates, Earth Planet. Sci. Lett., 48, 42-52.

Jelsma, H. A., and P. H. G. M. Dirks (2002), Neoarchean Tectonic Evolution of the Zimbabwe Craton, in The Early Earth: Physical, Chemical and Biological Development, edited by C. Fowler et al., Geol. Soc. Spec. Publ., 199, 183-211.

Jiménez-Munt, I., M. Fernàndez, E. Saura, J. Vergés, and D. Garcia-Castellanos (2012), 3D lithospheric structure and regional/residual Bouguer anomalies in the Arabia-Eurasia collision (Iran), Geophys. J. Int., 190(3), 1311-1324.

Jones, M. Q. W. (1988), Heat flow in the Witwatersrand Basin and environs and its significance for the South African shield geotherm and lithosphere thickness, J. Geophys. Res., 93, 3243-3260.

Jones, S. M., B. Lovell, and A. G. Crosby (2012), Comparison of modern and geological observations of dynamic support from mantle convection, J. Geol. Soc. London, 169(6), 745-758.

Kadima, E., D. Delvaux, S. N. Sebagenzi, L. Tack, S. M. Kabeya (2011), Structure and geological history of the Congo Basin: an integrated interpretation of gravity, magnetic and reflection seismic data, Basin Res., 23, 499–527, doi:10.1111/j.1365-2117.2011.00500.x.

Keranen, K. M., S. L. Klemperer, J. Julia, J. F. Lawrence, and A. A. Nyblade (2009), Low lower crustal velocity across Ethiopia: Is the Main Ethiopian Rift a narrow rift in a hot craton?, Geochem. Geophys. Geosyst., 10, Q0AB01, doi:10.1029/2008GC002293.

Kgaswane, E. M., A. A. Nyblade, J. Julia, P. H. G. M. Dirks, R. J. Durrheim, and M. E. Pasyanos (2009), Shear wave velocity structure of the lower crust in southern Africa: evidence for compositional heterogeneity within Archaean and Proterozoic terrains, J. Geophys. Res., 114, B12304.

Kgaswane, E. M., A. A. Nyblade, R. J. Durrheim, J. Julia, P. H. G. M. Dirks, and S. J. Webb (2012), Shear wave velocity structure of the Bushveld Complex, South Africa, Tectonophysics, 554, 83-104.

King, S. D., and D. L. Anderson (1995), An alternative mechanism to flood basalt formation, Earth Planet. Sci. Lett., 136, 269-279.

King, S. D., and J. Ritsema (2000), African hotspot volcanism: small-scale convection in the upper mantle beneath cratons, Science, 290, 1137-1140.

Klingelhoefer, F., C. Labails, E. Cosquer, S. Rouzo, L. Geli, D. Aslanian, L. L. Olivet, M. Sahabi, H. Nouze, and P. Unternehr (2009), Crustal structure of the SW-Moroccan margin from wide-angle and reflection seismic data (the DAKHLA experiment) part A: Wide-angle seismic models, Tectonophysics, 468(1-4), 63-82.

Kobussen, A. F., W. L. Griffin, S. Y. O'Reilly, and S. R. Shee (2008), Ghosts of lithospheres past: Imaging an evolving lithospheric mantle in Southern Africa, Geology, 36, 515-518.

Koehn, D, K. Aanyu, S. Haines, and T. Sachau (2008), Rift nucleation, rift propagation and the creation of basement micro-plates within active rifts, Tectonophysics, 458, 105-116, doi:10.1016/j.tecto.2007.10.003.

König, M., and W. Jokat (2010), Advanced insights into magmatism and volcanism of the Mozambique Ridge and Mozambique Basin in the view of new potential field data, Geophys. J. Int., 180, 158-180.

Kokonyangi, J., A. B. Kampunzu, R. Armstrong, M. Yoshida, T. Okudaira, M. Arima, and D. A. Ngulube (2006), The Mesoproterozoic Kibaridebelt (Katanga, SED. R. Congo), J. Afr. Earth Sci.,46, 1-35.

Kosarian, M. (2006), Lithospheric structure of North Africa and western Eurasia, PhD thesis, The Pennsylvania State University.

KRISP WORKING GROUP (1987), Structure of the Kenya rift from seismic refraction, Nature, 325, 239-242.

Kröner, A., and R. J. Stern (2004), Africa: Pan-African orogeny, in Encyclopedia of Geology, edited by R. Selley et al., Elsevier, 1-12.

Kumar, N., H. Zeyen, and A. P. Singh (2014), 3D Lithosphere density structure of southern Indian shield from joint inversion of gravity, geoid and topography data, J. Asian Earth Sci. 89, 98-107.

Kwadiba, M. T. O. G., C. Wright, E. M. Kgaswane, R. E. Simon, and T. K. Nguuri (2003), Pn arrivals and lateral variations of Moho geometry beneath the Kaapvaal Craton, Lithos, 71, 393-411.

Lachenbruch, A. H., and P. Morgan (1990), Continental extension, magmatism and elevation; formal relations and rules of thumb, Tectonophysics, 174, 39-62.

Laske, G., and G. Masters (1997), A global digital map of sediment thickness, Eos Trans. AGU 78, F483.

Laske, G., G. Masters, Z. Ma, and M. Pasyanos (2013), Update on CRUST1.0 a 1-degree global model of Earth's crust, Geophys. Res. Abstracts, Abstract EGU2013-2658.

Last, R. J., A. A. Nyblade, C. A. Langston, and T. J. Owens (1997), Crustal structure of the east African plateau from receiver functions and Rayleigh wave phase velocities, J. Geophys. Res., 102, 24469-24484.

Lebedev, S., and R. D. van der Hilst (2008), Global upper-mantle tomography with the automated multimode inversion of surface and S-wave forms, Geophys. J. Int., 173, 505-518.

Le Stunff, Y., and Y. Ricard (1995), Topography and geoid due to lithospheric mass anomalies, Geophys. J. Int., 122(3), 982-990, doi:10.1111/j.1365-246X.1995.tb06850.x.

Li, A., and K. Burke (2006), Upper mantle structure of southern Africa from Rayleigh wave tomography, J. Geophys. Res., 111, B10303.

Lindeque, A. S., T. Ryberg, J. Stankiewicz, M. H. Weber, and M. J. de Witt (2007), Deep crustal seismic reflection experiment across the southern Karoo Basin, South Africa, S. Afr. J. Geol., 110(2-3), 419-438, doi:10.2113/gssajg.110.2-3.419.

Link, K., D. Koehn, M. G. Barth, K. Aanyu, and S. F. Foley (2010), Continuous cratonic crust between the Congo and Tanzania blocks in western Uganda, Int. J. Earth. Sci. (Geol Rundsch), 99, 1559-1573.

Lithgow-Bertelloni, C., and P. Silver (1998), Dynamic topography, plate driving forces, and the African superswell, Nature, 395, 269-272.

Lucassen, F., G. Franz, R. L. Romer, D. Pudlo, and P. Dulski (2008), Nd, Pb, and Sr isotope composition of Late Mesozoic to Quaternary intra-plate magmatism in NE-Africa (Sudan, Egypt): high-μ, signatures from the mantle lithosphere, Contrib. Mineral. Petr., 156(6), 765-784.

MacGregor, D. S, R. T. J. Moody, and D. D. Clark-Lowes (1998), Petroleum Geology of North Africa, Geol. Soc. Spec. Publ., 132, 7-68.

Maguire, P. K. H., C. J. Swain, R. Masotti, and M. A. Khan (1994), A crustal and uppermost mantle cross-sectional model of the Kenya Rift derived from seismic and gravity data, in Crustal and Upper Mantle structure of the Kenya Rift, edited by C. Prodehl et al., Tectonophysics, 236, 217-249.

Maguire, P. K. H., G. R. Keller, S. L. Klemperer, G. D. Mackenzie, K. Keranen, S. Harder, B. O'Reilly, H. Thybo, L. Asfaw, and M. Amha (2006), Crustal structure of the northern Main Ethiopian Rift from the EAGLE controlled-source survey; a snapshot of incipient lithospheric break-up, in The Afar Volcanic Province within the East African Rift System, edited by G. Yirgu et al., Geol. Soc. Spec. Publ., 259, 269-292.

Makris, J., A. Demnati, and J. Klussmann (1985), Deep seismic soundings in Morocco and a crust and upper mantle model deduced from seismic and gravity data, Ann. Geophys., 3, 369-380.

Mancilla, F., D. Stich, J. Morales, J. Julià, J. Diaz, A. Pazos, D. Córdoba, J. A. Pulgar, P. Ibarra, M. Harnafi, and F. Gonzalez-Lodeiro (2012), Crustal thickness variations in northern Morocco, J. Geophys. Res., 117, B02312.

Mancilla, F., G. Booth-Rea, D. Stich, J. V. Pérez-Peña, J. Morales, J. M. Azañón, R. Martín, and F. Giaconia (2015), Slab rupture and delamination under the Betics and Rif constrained from receiver functions, Tectonophysics, 663, 225-237.

Manighetti, I., P. Tapponnier, V. Courtillot, S. Gruszow, and P. Y. Gillot (1997), Propagation of rifting along the Arabia-Somalia plate boundary: The Gulfs of Aden and Tadjoura, J. Geophys. Res., 102, 2681-2710.

Mann, P., L. Gahagan, and M. B. Gordon (2003), Tectonic setting of the world's giant oil and gas fields, in Giant oil and gas fields of the decade 1990-1999, edited by M. T. Halbouty, AAPG Memoir, 78, 15-105.

McClusky, S., R. Reilinger, S. Mahmoud, D. Ben Sari, and A. Tealeb (2003), GPS constraints on Africa (Nubia) and Arabia plate motions, Geophys. J. Int., 155, 126-138.

McConnell, R. B. (1972), Geological development of the rift system of eastern Africa, Bull. Geol. Soc. Am., 83, 2549-2572.

McKenzie, D. P. (1978), Some remarks on the development of sedimentary basins, Earth Planet. Sci. Lett., 40, 25-32.

McKenzie, G. D., H. Thybo, and P. K. H. Maguire (2005), Crustal velocity structure across the Main Ethiopian Rift: Results from two-dimensional wide-angle seismic modeling, Geophys. J. Int., 162, 994-1006.

McNutt, M. K. (1998), Superswells, Rev. Geophys., 36(2), 211-244, doi:10.1029/98RG00255.

Mechie, J., K. Abu-Ayyash, Z. Ben-Avraham, R. El-Kelani, A. Mohsen, G. Rümpker, J. Saul, and M. Weber (2005), Crustal shear velocity structure across the Dead Sea Transform from two-dimensional modeling of DESERT project explosion seismic data, Geophys. J. Int. 160, 910-924.

Meier, U., A. Curtis, and J. Trampert (2007), Global crustal thickness from neural network inversion of surface wave data, Geophys. J. Int., 169, 706-722.

Meyers, J. B., B. R. Rosendahl, C. G. A. Harrison, and Z. D. Ding (1998), Deep-imaging seismic and gravity results from offshore Cameroon Volcanic Line and speculation of African hot-lines, Tectonophysics, 284, 31-63.

Mériaux, C. A., J. C. Duarte, S. S. Duarte, W. P. Schellart, Z. Chen, F. Rosa, J. Mata, and P. Terrinha (2015), Capture of the Canary mantle plume material by the Gibraltar arc mantle wedge during slab rollback, Geophys. J. Int., 201(3), 1717-1721.

Midzi, V., and L. Ottemöller (2001), Receiver function structure beneath three Southern Africa seismic broadband stations, Tectonophysics, 339, 443-454.

Milani, E. J., and De Wit. (2008), Correlations between the classic Parana' and Cape-Karoo sequences of South America and southern Africa and their basin infills flanking the Gondwanides: du Toit revisted, in West Gondwana: Pre-Cenozoic Correlations Across the South Atlantic Region, edited by R. J. Pankhurst et al., Geol. Soc. Publ., 294, 319-342.

Milesi, J. P., D. Frizon de Lamotte, G. de Kock, and F., Toteu (2010), Tectonic map of Africa, 1:10 000 000 scale. CCGM-CGMW, Paris.

Miller, M. S., A. A. Allam, T. W. Becker, J. F. Di Leo, and J. Wookey (2013), Constraints on the tectonic evolution of the westernmost Mediterranean and northwestern Africa from shear wave splitting analysis, Earth Planet. Sci. Lett., 375, 234-243.

Miller, M. S., L. O'Driscoll, A. J. Butcher, and C. Thomas (2015), Imaging Canary Island hotspot material beneath the lithosphere of Morocco and southern Spain, Earth Planet. Sci. Lett., 431,186-194.

Mohr, P., and B. Zanettin (1988), The Ethiopian flood basalt province, in Continental Flood Basalts, edited by J. D. Macdougall, Kluwer, Dordrecht, 63-110.

Molnar, P., P. C. England, and C. H. Jones (2015), Mantle dynamics, isostasy, and the support of high terrain, J. Geophys. Res. Solid Earth, 120, 1932-1957.

Mooney, W. D., G. Laske, and G. Masters (1998), CRUST-5.1: a global crustal model at 5º x 5º, J. Geophys. Res., 103, 727-747.

Morelli, C., and R. Nicolich (1990), A cross section of the lithosphere along the European Geotraverse Southern Segment (from the Alps to Tunisia), Tectonophysics, 176, 229-243.

Morley, C. K. (1999), Influence of preexisting fabrics on rift structure, in Geoscience of Rift Systems Evolution of East Africa, edited by C. K. Morley, AAPG Studies in Geology, 44, 151-160.

Moucha, R., and A. M. Forte (2011), Changes in African topography driven by mantle convection, Nature, 4(10), 707-712.

Nair, S. K., S. S. Gao, K. H. Liu, and P. G. Silver (2006), Southern African crustal evolution and composition: constraints from receiver function studies, J. Geophys. Res., 111, B02304.

Nataf, H. C., and Y. Ricard (1996), 3SMAC: an a priori tomographic model of the upper mantle based on geophysical modeling, Phys. Earth. Planet. Int., 95, 101-122.

Ngako, V., E. Njonfang, F. T. Aka, P. Affaton, and J. M. Nnange (2006), The North-South Paleozoic to Quaternary trend of alkaline magmatism from Niger-Nigeria to Cameroon: complex interaction between hotspots and Precambrian faults, J. Afr. Earth Sci., 45, 241-256.

Nguuri, T. K., J. Gore, D. E. James, S. J. Webb, C. Wright, T. G. Zengeni, Gwavava, J. A. Snoke, and Kaapvaal Seismic Group (2001), Crustal structure beneath southern Africa and its implications for the formation and evolution of the Kaapvaal and Zimbabwe cratons, Geophys. Res. Lett., 28, 2501-2504.

Ni, S., E, Tan, M. Gurnis, and D. Helmberger (2002), Sharp sides to the African superplume, Science, 296, 1850-1852.

Niu, F., and D. E. James (2002), Fine structure of the lowermost crust beneath the Kaapvaal Craton and its implications for crustal formation and evolution, Earth Planet. Sci. Lett., 200, 121-130.

Nocquet, J. M., and E. Calais (2003), The crustal velocity field in Western Europe from permanent GPS array solutions, 1996-2001, Geophys. J. Int., 154, 72-88.

Nolet, G. R., R. Montelli, G. Masters, F. A. Dahlen, and S. Hung, (2003), Finite frequency tomography shows a variety of plumes, Geophys. Res. Abstr., 5, 03146.

Nyblade, A. A., and S. W. Robinson (1994), The African Superswell, Geophys. Res. Lett. 21, 765-768.

Nyblade, A. A., and C. A. Langston (2002), Broadband seismic experiments probe the East African Rift, Eos Trans. AGU, 83, 405-408, doi:10.1029/2002EO000296.

Nyblade, A. A., and N. Sleep (2003), Long lasting epeirogenic uplift from mantle plumes and the origin of the Southern African Plateau, Geochem. Geophys. Geosyst., 4(12), 1105.

Okereke, C. S. (1984), A gravity study of the lithospheric structure beneath the West Africa rift system in Nigeria and Cameroon, PhD Thesis, Univ. of Leeds, UK, 272p.

Oldenburg, D.W. (1974), Inversion and interpretation of gravity anomalies, Geophysics, 39, 526-536.

Pail, R., H. Goiginger, W. D. Schuh, E. Höck, J. M. Brockmann, T. Fecher, T. Gruber, T. Mayer-Gürr, J. Kusch, A. Jgi, and D. Rieser (2010), Combined satellite gravity field model GOCO01S derived from GOCE and GRACE, Geophys. Res. Lett., 37, L20314.

Palomeras, I., S. Thurner, A. Levander, K. Liu, A. Villaseñor, R. Carbonell, and M. Harnafi (2014), Finite-frequence Rayleigh wave tomography of the western Mediterranean: Mapping its lithospheric structure, Geochem. Geophys. Geosyst., 15, 140-160.

Parker, R. L. (1973), The rapid calculation of potential anomalies, Geophys. J. R. Astron. Soc., 31, 447-455.

Parsiegla, N., J. Stankiewicz, K. Gohl, T. Ryberg, and G. Uenzelmann-Neben (2009), Southern African continental margin: Dynamic processes of a transform margin, Geochem. Geophys. Geosyst., 10, Q03007, doi:10.1029/2008GC002196.

Pasyanos, M. E., and A. A. Nyblade (2007), A top to bottom lithospheric study of Africa and Arabia, Tectonophysics, 444, 27-44.

Pasyanos, M. E. (2010), Lithospheric thickness modeled from long period surface wave dispersion, Tectonophysics, 481, 38-50, doi:10.1016/j.tecto.2009.02.023.

Pasyanos, M. E., T. G. Masters, G. Laske, and Z. Ma (2014), LITHO1.0: An updated crust and lithospheric model of the Earth, J. Geophys. Res., 119(3), 2153-2173, doi:10.1002/2013JB010626.

Pavlis, N. K., S. A. Holmes, S. C. Kenyon, and J. K. Factor (2012), The development and evaluation of the Earth Gravitational Model 2008 (EGM2008), J. Geophys. Res., 117, B04406.

Pearson, D. G., R. W. Carlson, S. B. Shirey, F. R. Boyd, and P. H. Nixon (1995), Stabilisation of Archaean lithospheric mantle: A Re-Os isotope study of peridotite xenoliths from the Kaapvaal craton, Earth Planet. Sci. Lett., 15, 341-357.

Pérez-Gussinyé, M., M. Metois, M. Fernàndez, J. Vergés, J. Fullea, and A. R. Lowry (2009), Effective elastic thickness of Africa and its relationship to other proxies for lithospheric structure and surface tectonics, Earth Planet. Sci. Lett., 287(1-2), 152-167.

Pik, R., B. Marty, and D. R. Hilton (2006), How many mantle plumes in Africa? The geochemical point of view, Chem. Geol., 226, 100-114.

Plomerova, J., D. Kouba, and V. Babuska (2002), Mapping the lithosphere - asthenosphere boundary through changes in surface-wave anisotropy, Tectonophysics, 358, 175-185.

Priestley, K. (1999), Velocity structure of the continental upper mantle: evidence from southern Africa, Lithos, 48, 45-56.

Priestley, K., and D. McKenzie (2006), The thermal structure of the lithosphere from shear wave velocities, Earth Planet. Sci. Lett., 244, 285-301.

Priestley, K., D. McKenzie, E. Debayle, and S. Pilidou, (2008), The African upper mantle and its relationship to tectonics and surface geology, Geophys. J. Int., 175, 1108-1126.

Priestley, K., and F. Tilmann (2009), Relationship between the upper mantle high velocity seismic lid and the continental lithosphere, Lithos, 109(1-2), 112-124.

Priestley, K., and D. McKenzie (2013), The relationship between shear wave velocity, temperature, attenuation and viscosity in the shallow part of the mantle, Earth Planet. Sci. Lett., 381, 78-91.

Prodehl, C., B. Jacob, H. Thybo, E. Dindi, and R. Stangl (1994), Crustal structure on the northeastern flank of the Kenya rift, in: Crustal and Upper Mantle Structure of the Kenya Rift, edited by C. Prodehl et al., Tectonophysics, 236, 271-290.

Prodehl, C., J. R. R. Ritter, M. Mechie, G. R. Keller, M. A. Khan, B. Jacob, K. Fuchs, I. O. Nyambok, J. D. Obel, and D. Riaroh (1997), The KRISP 93/94 lithospheric investigations of southern Kenya-The experiments and their main results, Tectonophysics, 278, 121-147.

Reguzzoni, M., D. Sampietro, and F. Sans (2013), Global Moho from the combination of the CRUST2.0 model and GOCE data, Geophys. J. Int., 195(1), 222-237.

Reid, A. B., J. Ebbing, and S. J. Webb (2012), Comment on ‘A crustal thickness map of Africa derived from a global gravity field model using Euler deconvolution’ by Tedla, G. E., M. van der Meijde, A. A. Nyblade and F. D. van der Meer, Geophys. J. Int., 189(3), 1217-1222, doi:10.1111/j.1365-246X.2012.05353.x.

Reusch, A. M., A. A. Nyblade, D. A. Wiens, P. J. Shore, B. Ateba, C. T. Tabod, and J. M. Nnange (2010), Upper mantle structure beneath Cameroon from body wave tomography and the origin of the Cameroon Volcanic Line, Geochem. Geophys. Geosyst., 11, Q10W07.

Ricard, Y., M. Richards, C. Lithgow-Bertelloni, and Y. Le Stuenff (1993), A geodynamic model of mantle density heterogeneity, J. Geophys. Res., 98, 21895-21909.

Rihm, R., J. Makris, and L. Möller (1991a), Seismic surveys in the northern Red Sea: asymmetric crustal structure, Tectonophysics, 198, 279-295.

Rihm, R., J. Makris, Y. A. Izzeldin, M. Bobsien, K. Meier, P. Junge, T. Noman, and W. Warsi (1991b), Contrasting structural styles of the eastern and western margins of the southern Red Sea: the 1988 SONNE experiment, Tectonophysics, 198, 329-353.

Ring, U. (1994), The influence of preexisting crustal anisotropies on the evolution of the Cenozoic Malawi rift (East African rift system), Tectonics, 13, 313-326.

Ritsema, J., H. J. van Heijst, and J. H. Woodhouse (1999), Complex shear velocity structure imaged beneath Africa and Iceland, Science, 286, 1925-1928.

Ritsema J., and H. J. van Heijst (2000), New seismic model of the upper mantle beneath Africa, Geology, 28, 63-66.

Ritsema, J., and R. Allen (2003), The elusive mantle plume, Earth Planet. Sci. Lett., 207, 1-12.

Robert, A., M. Fernàndez, I. Jiménez-Munt, and J. Vergés (2015), Lithospheric structures in Central Eurasia derived from elevation, geoid anomaly and a thermal analysis, Geol. Soc. Spec. Publ., 427, doi.org/10.1144/SP427.10.

Roberts, D. G., and A. W. Bally (2012), Regional geology and tectonics: Phanerozoic passive margins, cratonic basins and global tectonic maps, Burlington: Elsevier Science.

Rogers, N., R. McDonald, J. G. Fitton, R. George, M. Smith, and B. Barreiro, (2000), Two mantle plumes beneath the East African rift system: Sr, Nd and Pb isotope evidence from Kenya Rift basalts, Earth Planet. Sci. Lett., 176, 387-400.

Rooney, T. O., B. B. Hanan, D. W. Graham, T. Furman, J. Blichert-Toft, and J. G. Schilling (2012), Upper Mantle Pollution during Afar Plume-Continental Rift Interaction, J. Petrol., 53, 365-389.

Root, B. C., W. van der Wal, P. Novák, J. Ebbing, and L. L. A. Vermeersen (2014), Glacial isostatic adjustment in the static gravity field of Fennoscandia, J. Geophys. Res. Solid Earth, 120, 503-518, doi:10.1002/2014JB011508.

Rosenbaum, G., and G. S. Lister (2004), Neogene and Quaternary rollback evolution of the Tyrrhenian Sea, the Apennines, and the Sicilian Maghrebides, Tectonics, 23, TC1013.

Royer, J. Y., and M. F. Coffin (1992), Jurassic to Eocene plate tectonic reconstructions in the Kerguelen plateau region, Proc. Ocean Drill. Program Sci. Results, 120, 917-928.

Rychert, C. A., and P. M. Shearer, P.M (2009), A global view of the lithosphere-asthenosphere boundary, Science, 324, doi:10.1126/science.1169754.

Sandvol, E., D. Seber, A. Calvert, and M. Barazangi, (1998), Grid search modeling of receiver functions: Implications for crustal structure in the Middle East and North Africa, J. Geophys. Res., 103, 26899-26917.

Sandwell, D. T., and W. H. F. Smith (1997), Marine gravity anomaly from Geosat and ERS 1 satellite altimetry, J. Geophys. Res., 102(B5), 10039-10054.

Savage, B., and P. G. Silver (2008), Evidence for a compositional boundary within the lithospheric mantle beneath the Kalahari craton from S receiver functions, Earth Planet. Sci. Lett., 272, 600-609.

Schilling, J. G. (1973), Afar mantle plume: rare earth evidence, Nature, 242, 2-5.

Schoene, B., M. J. deWit, and S. A. Bowring (2008), Mesoarchean assembly and stabilization of the eastern Kaapvaal craton: A structural-thermochronological perspective, Tectonics, 27, TC5010.

Sebai, A., E. Stutzmann, J. P. Montagner, D. Sicilia, and E. Beucler (2006), Anisotropic structure of the African upper mantle from Rayleigh and Love wave tomography, Phys. Earth Planet. Int., 155, 48-62.

Sengör, A. M. C., and K. Burke (1978), Relative timing of rifting and volcanism on Earth and its tectonic implications, Geophys. Res. Lett., 5, 419-421, doi:10.1029/GL005i006p00419.

Shang, C. K., G. Morteani, M. Satir, and H. Taubald (2010), Neoproterozoic continental growth prior to Gondwana assembly: constraints from zircon-titanite geochronology, geochemistry and petrography of ring complex granitoids, Sudan, Lithos, 118, 61-81.

Shapiro, N. M., and M. H. Ritzwoller (2002), Monte-Carlo inversion for a global shear velocity model of the crust and upper mantle, Geophys. J. Int., 151(1), 88-105.

Simiyu, S. M., and G. R. Keller (1997), An integrated analysis of lithospheric structure across the East African plateau based on gravity anomalies and recent seismic studies, Tectonophysics, 278, 291-313.

Simmons, N. A., A. M. Forte, and S. P. Grand (2007), Thermo-chemical structure and dynamics of the African super-plume, Geophys. Res. Lett., 34, L02301.

Simmons, N., A. Forte, and S. P. Grand (2009), Joint seismic, geodynamic and mineral physical constraints on three-dimensional mantle heterogeneity: Implications for the relative importance of thermal versus compositional heterogeneity, Geophys. J. Int., 177, 1284-1304.

Soller, D. R., R. D. Ray, and R. D. Brown (1982), A new global crustal thickness model, Tectonics, 1, 125-149.

Spada, M., I. Bianchi, E. Kissling, A. Piana Agostinetti, and S. Wiemer (2013), Combining controlled-source seismology and receiver function information to derive 3-D Moho topography for Italy, Geophys. J. Int., 194(2), 1050-1068.

Spakman, W., and R. Wortel (2004), A tomographic view on western Mediterranean geodynamics, in The Transmed Atlas, the Mediterranean Region from Crust to Mantle, edited by W. Cavazza et al., 31-52, Springer, Berlin.

Spieker, K., I. Wölbern, C. Thomas, M. Harnafi, and L. E. Moudnib (2014), Crustal and upper mantle structure beneath the western Atlas Mountains in SW Morocco derived from receiver functions, Geophys. J. Int., 198(3), 1474-1485.

Stankiewicz, J., T. Ryberg, N. Parsiegla, K. Gohl, R. Trumbull, and M. Weber (2008), Crustal structure of the Southern Margin of the African Plate: Results from Geophysical Experiments, J. Geophys. Res., 113, B10313.

Stuart, G. W., and T. G. Zengeni (1987), Seismic crustal structure of the Limpopo mobile belt, Tectonophysics, 144, 323-335.

Stuart, G. W., I. D. Bastow, and C. J. Ebinger (2006), Crustal structure of the Northern Main Ethiopian rift from receiver function studies, in The Afar Volcanic Province within the East African Rift System, edited by G. Yirgu et al., Geol. Soc. Spec. Publ., 259, 253-267.

Tedla, G. E., M. van der Meijde, A. A. Nyblade, and F. van der Meer (2011), A crustal thickness map of Africa derived from a global gravity field model using Euler deconvolution, Geophys. J. Int., 187, 1-9.

Teixell A., P. Ayarza, H. Zeyen, M. Fernàndez, and M. L. Arboleya (2005), Effects of mantle upwelling in a compressional setting: the Atlas Mountains of Morocco, Terra Nova, 17, 456-461.

Tenzer R., W. Chen, D. Tsoulis, M. Bagherbandi, L. E. Sjöberg, P. Novák, and S. Jin (2015), Spectral and spatial characteristics of the refined CRUST1.0 gravity field, Surv. Geophys., 36, 139-165.

Thorpe, R. S. and K. Smith (1974), Distribution of Cenozoic volcanism in Africa, Earth Planet. Sci. Lett., 22, 91- 95.

Tokam, A. P. K., C. T. Tabod, A. A. Nyblade, J. Julià, D. A. Wiens, and M. E. Pasyanos (2010), Structure of the crust beneath Cameroon, West Africa, from the joint inversion of Rayleigh wave group velocities and receiver functions, Geophys. J. Int., 183(2), 1061-1076.

Torne, M., M. Fernàndez, J. Vérges, C. Ayala, M. C. Salas, I. Jimenez-Munt, and G. G. Buffet (2015), Crustal and mantle lithosphere structure from potential field and thermal analysis, Tectonophysics, 663, 419-433.

Tugume, F., A. A. Nyblade, J. Julia, and M. van der Meijde (2013), Crustal shear wave velocity structure and thickness for Archean and Proterozoic terranes in Africa and Arabia from modeling receiver functions, surface wave dispersion, and satellite gravity data, Tectonophysics, 609, 250-266.

Turcotte, D. L., and G. Schubert (2002), Geodynamics: Applications of Quantum Physics to Geological Problems, John Wiley and Sons, New York, 456p.

van der Meijde M., S. van der Lee, and D. Giardini (2003), Crustal structure beneath broad-band seismic stations in the Mediterranean region, Geophys. J. Int., 152, 729-739, doi:10.1046/j.1365-246X.2003.01871.x.

van der Meijde, M., and A. A. Nyblade (2014), Reply to “Comment on ‘A crustal thickness map of Africa derived from a global gravity field model using Euler deconvolution”’. In: Geophys. J. Int., 196(1), 96-99, doi:10.1093/gji/ggt450.

van der Meijde, M., I. E. A. M. Fadel, P. Ditmar, and M. Hamayun (2015), Uncertainties in crustal thickness models for data sparse environments: A review for South America and Africa, J. Geodyn., 84, 1-18.

Vergés, J., and F. Sàbat (1999), Constraints on the Neogene Mediterranean kinematic evolution along a 1000 km transect from Iberia to Africa, in The Mediterranean Basins: Tertiary Extension within the Alpine Orogen, edited by B. Durand et al., Geol. Soc. Spec. Publ., 156, 63-80.

Vergés, J., and M. Fernàndez (2012), Tethys-Atlantic interaction along the Iberia-Africa plate boundary: The Betic-Rif orogenic system, Tectonophysics, 579, 144-172.

Vilà, M., M. Fernàndez, and I. Jiménez-Munt (2010), Radiogenic heat production variability of some common lithological groups and its significance to lithospheric thermal modeling, Tectonophysics, 490, 152-164.

Villeneuve, M. (2005), Paleozoic basins in West Africa and the Mauritanide thrust belt, J. Afr. Earth. Sci., 43, 166-195.

Vinnik, L., S. Oreshin, G. Kosarev, S. Kiselev, and L. Makeyeva (2009), Mantle anomalies beneath southern Africa: Evidence from seismic S and P receiver functions, Geophys. J. Int., 179(1), 279-298.

Visser, J. N. J. (1997), A review of the Permo-Carboniferous glaciation in Africa, in Deglaciation and Global Changes: Quaternary, Permo-Carboniferous and Proterozoic, edited by I. P. Martini, Oxford Univ. Press, 169-191.

Waldhauser, F., E. Kissling, J. Ansorge, and S. Mueller (1998), Three-dimensional interface modelling with two-dimensional seismic data: the Alpine crust-mantle boundary, Geophys. J. Int., 135, 264-278.

Wang, Y., L. Wen, and D. Weidner (2008), Upper mantle SH- and P-velocity

structures and compositional models beneath southern Africa, Earth Planet. Sci. Lett., 267, 596-608.

Watts, A. B. (2001), Isostasy and Flexure of the Lithosphere, Cambridge, Cambridge University Press, 458p.

Webb, S. J., R. G. Cawthorn, T. Nguuri, and D. James (2004), Gravity modeling of Bushveld Complex connectivity supported by Southern African Seismic Experiment results, S. Afr. J. Geol., 107, 207-218.

Weeraratne, D., D. Forsyth, K. Fischer, and A. A. Nyblade (2003), Evidence for an upper mantle plume beneath the Tanzanian craton from Rayleigh wave tomography, J. Geophys. Res., 108(B9), 2427, doi:10.1029/2002JB002273.

Wigger, P., G. Asch, P. Giese, W. D. Heinsohn, S. O. El Alami, and F. Ramdani (1992), Crustal structure along a traverse across the Middle and High Atlas mountains derived from seismic refraction studies, Geol. Rundschau, 81(1), 237-248.

Willmore, P. L., A. L. Hales, and P. G. Gane (1952), A seismic investigation of crustal structure in the western Transvaal, Bull. Seis. Soc. Am., 42, 53-80.

Wilson, M., and R. Guiraud (1992), Magmatism and Rifting in Western and Central Africa, from Late Jurassic to Recent Times, Tectonophysics, 213, 203-225.

Wittlinger, G., and V. Farra (2007), Converted waves reveal a thick and layered tectosphere beneath the Kalahari super-craton, Earth Planet. Sci. Lett., 254, 404-415.

Wölbern, I., G. Rümpker, A. Schumann, and A. Muwanga (2010), Crustal thinning beneath the Rwenzori region, Albertine rift, Uganda, from receiver-function analysis, Int. J. Earth Sci., 99, 1545-1557.

Woodhouse, J. H., and A. M. Dziewonski (1984), Mapping the upper mantle: Three dimensional modeling of Earth structure by inversion of seismic waveforms, J. Geophys. Res., 89, 5953-5986.

Wopfner, H. (2002), Tectonic and climatic events controlling deposition in Tanzanian Karoo basins, J. Afr. Earth. Sci., 34, 167-177.

Wortel, M. J. R., and W. Spackman (2000), Subduction and slab detachment in the Mediterranean-Carpathian region, Science, 290, 1910-1917.

Wright, J. A., and J. Hall (1990), Deep seismic profiling in the Nosop Basin, Botswana: cratons, mobile belts and sedimentary basins, Tectonophysics, 173, 333-343.

Youssof, M., H. Thybo, I. M. Artemieva, and A. Levander (2013), Moho depth and crustal composition in Southern Africa, Tectonophysics, 609, 267-287.

Zeyen, H., P. Ayarza, M. Fernàndez, and A. Rimi (2005), Lithospheric structure under the western African-European plate boundary: A transect across the Atlas Mountains and the Gulf of Cadiz, Tectonics, 24, doi:10.1029/2004TC001639.

Zhao, D. (2001), Seismic structure and origin of hotspots and mantle plumes, Earth Planet. Sci. Lett., 192, 251-265.

Zhou, Y., G. Nolet, F. A. Dahlen, and G. Laske (2006), Global upper-mantle structure from finite-frequency surface-wave tomography, J. Geophys. Res.,111, B04304, doi:10.1029/2005JB003677.